J. Fluid Mech. (2010), *vol.* 644, *pp.* 123–163.
doi:10.1017/S0022112009992102

The long range persistence of wakes behind a row of roughness elements

M. E. GOLDSTEIN[1]†, ADRIAN SESCU[2], PETER W. DUCK[3] AND MEELAN CHOUDHARI[4]

[1]National Aeronautics and Space Administration, Glenn Research Center, Cleveland, OH 44135, USA
[2]University of Toledo, Department of Mechanical Industrial & Manufacturing Engineering, Toledo, OH 43606, USA
[3]University of Manchester, School of Mathematics, Manchester M13 9PL, UK
[4]National Aeronautics and Space Administration, Langley Research Center, Hampton, VA 23681, USA

(Received 23 March 2009; revised 8 September 2009; accepted 9 September 2009)

We consider a periodic array of relatively small roughness elements whose spanwise separation is of the order of the local boundary-layer thickness and construct a local asymptotic high-Reynolds-number solution that is valid in the vicinity of the roughness. The resulting flow decays on the very short streamwise length scale of the roughness, but the solution eventually becomes invalid at large downstream distances and a new solution has to be constructed in the downstream region. This latter result shows that the roughness-generated wakes can persist over very long streamwise distances, which are much longer than the distance between the roughness elements and the leading edge. Detailed numerical results are given for the far wake structure.

1. Introduction

Surface roughness can influence laminar turbulent transition in several different ways, depending on the nature of the underlying boundary-layer flow, as well as on the height and spatial distribution of the roughness elements. The primary effects of the roughness may be characterized by its impact on receptivity and linear amplification in cases where transition occurs via the well-known paradigm of receptivity and linear growth followed by a sequence of nonlinear events leading to laminar breakdown. Small-amplitude roughness elements with an appropriate wavenumber spectrum may, for example, serve to 'scatter' free-stream unsteadiness into travelling wave instabilities (Goldstein 1985) or to act as a direct source of stationary vortex instabilities such as Görtler vortices and stationary crossflow modes (Denier, Hall & Seddougui 1991; Choudhari & Duck 1996). Sufficiently tall elements can also produce $O(1)$ changes in the underlying base flow, but the dominant instability mechanisms can remain unchanged (with only the underlying instability growth rates being modified), even when the basic flow is substantially altered by the surface roughness. This scenario often applies to two-dimensional roughness distributions, i.e. surface height variations that are primarily confined to the direction of the mean pressure gradient.

† Email address for correspondence: Marvin.E.Goldstein@nasa.gov

In other cases, typically involving three-dimensional variations in surface geometry, the surface roughness may introduce more substantial changes in the boundary-layer instability mechanisms. A dramatic example of such changes is the onset of unsteady vortex shedding behind three-dimensional roughness elements in a low-speed boundary layer (Acarlar & Smith 1987; Klebanoff, Cleveland & Tidstrom 1992). An additional example involves the formation of stationary streaks within the wakes of discrete roughness elements in high-Mach-number boundary layers (Berry *et al.* 2001). The resulting flow can support highly unstable linear eigenmodes that are best characterized as streak instabilities (Choudhari, Li & Edwards 2009). Analogous streaks are also known to occur in low-speed boundary layers (Fransson *et al.* 2004), where, depending on the wavenumber and the amplitude of the streaks, they have been found to exert either a destabilizing or a stabilizing influence on the amplification of boundary-layer instabilities (Cossu & Brandt 2002; Fransson *et al.* 2005).

It is suspected that roughness-induced streaks also play a role in the *bypass* transition caused by distributed, three-dimensional surface roughness in linearly stable or, at most, weakly unstable boundary-layer flows. There is an additional class of flows where the presence of three-dimensional, distributed surface roughness leads to transition under conditions where the unperturbed boundary-layer flow is either stable or, at most, weakly unstable. In fact, it is well known that certain types of initial perturbations may undergo a transient algebraic growth prior to an eventual exponential decay even in linearly stable shear flows (Case 1960; Ellingson & Palm 1975; Landahl 1980). Recent work suggests that the maximum growth factors associated with certain optimal perturbations may be quite large, with the associated energy amplification ratio approaching a value of several thousand (Andersson, Berggren & Henningson 1999; Tumin & Reshotko 2001). The transient growth paradigm has, therefore, emerged as a possible explanation for the subcritical transition due to surface roughness. In fact, Reshotko & Tumin (2002) found that a semi-empirical transition prediction criterion based on optimal disturbance growth is able to correlate both of the major trends observed in transition measurements over rough axisymmetric nosetips, namely, the dependence of transition location on roughness height and the surface temperature. Given the success of this result, it seems important to understand the physical mechanisms related to potential disturbance growth in the wake flow behind the surface roughness.

It is well known that algebraic or non-modal growth usually arises from the 'lift-up' effect associated with spanwise varying displacement of a two-dimensional shear flow (Landahl 1980) and has been associated with the so called 'transient growth' that results from the non-normality of the linear stability operator (Trefethen *et al.* 1993). Non-normality implies that a suitable superposition of linearly stable eigenmodes may involve significant cancellation between the associated flow perturbations. The gradual weakening of the mutual cancellation is expected to result in a transient growth in disturbance amplitudes with increasing downstream distance. However, algebraic growth occurs over long streamwise length scales of the order of the streamwise variations in the underlying mean flow (i.e. non-parallel effects), which means, among other things, that the destructive interference characteristics cannot be sustained as the disturbances evolve downstream and that any strict asymptotic approach to the problem must include non-parallel flow effects at the lowest order of approximation. Optimal growth theory (Farrell 1988; Butler & Farrell 1992; Andersson *et al.* 1999; Luchini 2000; Tumin & Reshotko 2001; Levin & Henningson 2003) provides an upper bound on the algebraic amplification factors. According to this theory, the optimal initial conditions are associated with velocity perturbations resembling a

spanwise array of streamwise vortices – with the transient growth occurring as a result of these initial conditions evolving into streak-like motions that are dominated by perturbations in the streamwise velocity.

The actual relevance of optimal growth theory to boundary-layer transition is largely dependent on receptivity characteristics of the laminar boundary layer with the most important consideration being whether these characteristics allow such optimal (or near optimal) initial conditions to be realized in a natural disturbance environment. Transient growth of low-frequency boundary-layer disturbances due to weak to moderate free-stream turbulence has been documented in a number of experiments (Kendall 1985; Westin *et al.* 1994) and also predicted using theoretical models (Andersson *et al.* 1999; Leib, Wundrow & Goldstein 1999). The work by Leib *et al.* (1999) demonstrates the need to model the transient growth phenomenon as an inhomogeneous boundary value problem associated with a physically realizable forcing environment, rather than via the optimal growth formulation alone.

The analogous issue of whether initial conditions appropriate for near-optimal growth can also be seeded via three-dimensional surface roughness (and, if so, of what kind) has recently received considerable attention. Experimental studies predating the developments in optimal growth theory (Tani 1962; Kendall 1982; Gaster, Grosch & Jackson 1994) show that streak-like perturbations induced by isolated roughness elements can persist for large distances behind the element. The evolution of streak amplitudes behind a spanwise periodic array of elements has been measured in the recent experiments by White & Ergin (2003) and Fransson *et al.* (2004). Related computational studies (Choudhari & Fischer 2005) were able to reproduce the measured flow behaviour in these experiments and also provided further insights into the origin of transient growth behind the array and the highly suboptimal growth factors involved. A linear finite-Reynolds-number model for the perturbations behind the array of roughness elements was proposed by Tumin & Reshotko (2005). While certain qualitative aspects of the experimentally observed wake structure were captured by this model, the underlying assumptions were inherently inconsistent with the nonlinear dependence of measured disturbance amplitudes on the roughness height.

Despite the above-mentioned progress in understanding the near to far wake perturbations behind three-dimensional surface roughness, a number of key questions still remain unanswered, especially with regard to the scaling of streak amplitudes in terms of roughness geometry and flow Reynolds number, as well as the switchover from a linear behaviour at sufficiently small roughness heights to the nonlinear behaviour encountered in the experiments. In the past, high-Reynolds-number asymptotic methods have been successful in providing appropriate scaling laws and clarifying a number of key issues related to boundary-layer transition (e.g. Goldstein, 1985; Goldstein & Hultgren 1989; Leib *et al.* 1999). The present paper uses this approach to examine both linear and nonlinear perturbations due to a spanwise periodic array of relatively small roughness elements whose (spanwise) separation and plan form dimensions are of the order of the local boundary-layer thickness δ^* (figure 1).

While the analysis in this paper would apply to any arbitrary incompressible boundary layer with a non-zero wall shear with only minor modification, for definiteness, we only consider the incompressible flat plate boundary layer. The problem is formulated in § 2 and the local asymptotic high Reynolds number solution in the vicinity of the roughness is outlined in § 3. It is shown to have a double layer structure with the same scaling as in Choudhari & Duck (1996). An analogous

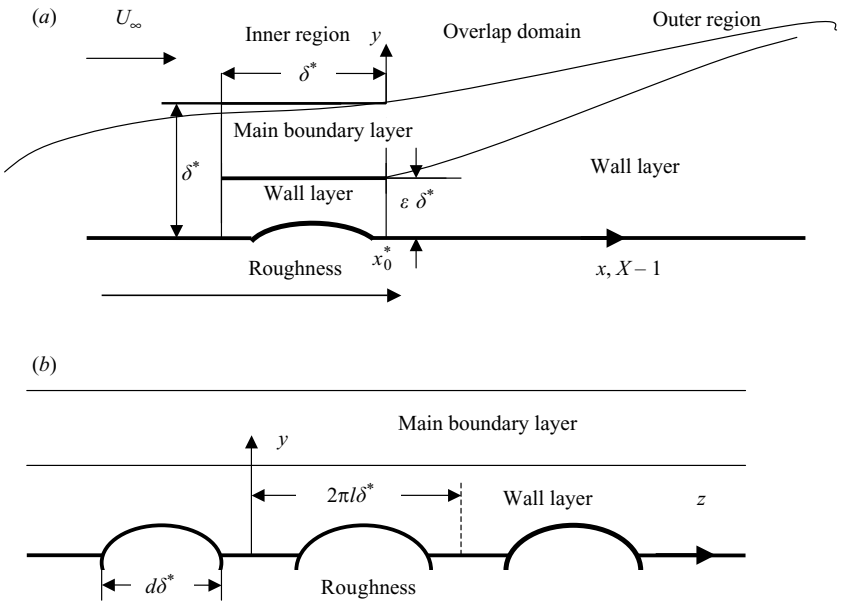

FIGURE 1. Boundary-layer flow structure: (*a*) side view, (*b*) cross-sectional view.

two-dimensional problem was studied by Smith (1973) and Smith *et al.* (1981). They show that the flow decays algebraically fast and eventually becomes linear far downstream (on the roughness scale δ^*) of the roughness. The Choudhari & Fischer (2005) simulations show that the spanwise variable components of the three-dimensional wakes initially undergo a very rapid decay in the vicinity of the roughness. It is, therefore, reasonable to assume that the flow is eventually governed by linear equations at sufficiently large streamwise distances behind the three-dimensional roughness elements being considered in the present paper – even when there is significant nonlinearity in the vicinity of the roughness – and that, as in the two-dimensional case and the three-dimensional linear case, the flow decays algebraically fast on the short streamwise length scale δ^* of the roughness. Numerical solutions to the full nonlinear equations are used to verify that this actually occurs. The analysis shows that the decay rate exponent α of the spanwise variable component of the pressure is equal to $8/3$ when the nonlinear terms are negligible, and no slower than $5/3$ when they are not.

But the analysis also shows that the first-order terms (in the expansion parameter $\varepsilon \equiv R^{-1/6}$, where R is the length Reynolds number at the downstream location x_0^* of the roughness) eventually become of the same order as the zeroeth-order terms – causing the solution to become invalid at $O(x_0^*)$ distance downstream of the roughness array (§4). The problem, therefore, has to be rescaled and a new solution has to be constructed in this downstream region. This is described in §5, where it is also shown that the downstream 'outer' solution can be matched (in the strict asymptotic sense) onto the local 'inner' solution. The former 'outer' solution, which is determined by the linearized boundary region (LBR) equations (Kemp 1951), shows that the roughness-generated wakes can actually persist over very long streamwise distances, which can be much longer than the distance x_0^* between the roughness elements and the leading edge. The general nonlinear solution involves considerable numerical computation,

but analytical results are obtained for the strictly linear problem (where the scaled roughness height $h \ll 1$) in § 6 and extensive numerical computations are also carried out for this case. The results and implications of the theory are discussed in § 8, where some detailed comparisons with the nonlinear results are given. They show that wake energies for the fully nonlinear case (corresponding to $O(1)$ scaled roughness heights) will be larger by a factor of $R = \varepsilon^{-6}$ than those in the strictly linear case. The surprising conclusion from this is that relatively mild nonlinearity ($h = O(1)$ or so) can have a much larger effect on the far wakes than on the near field flow in the vicinity of the roughness. This suggests an extreme sensitivity to initial conditions that is one of the more important characteristics of a chaotic flow.

2. Problem formulation and asymptotic scaling

As indicated in § 1, we consider an incompressible flat plate boundary layer that is perturbed by a spanwise periodic linear array of roughness elements. Significant disturbance growth is expected to occur when the spanwise length scale of the roughness, say $2\pi l\,\delta^*$, is equal to or somewhat larger than the local boundary-layer thickness $\delta^* \equiv x_0^*/\sqrt{R} = x_0^*\delta$ at the roughness location $x^* = x_0^*$, where $R \equiv x_0^* U_\infty/\nu^*$ is the Reynolds number based on x_0^* and the free-stream velocity U_∞ with ν^* being the kinematic viscosity and $\delta \equiv R^{-1/2} \gg 1$ being the scaled boundary-layer thickness. The emphasis in this paper is on more or less circular roughness elements with the same streamwise and spanwise scaling and it seems reasonable to require that the roughness be small enough to produce only local separation. It might then appear that the triple-deck structure would produce the distinguished scaling, but this is only true for two-dimensional flows. For the roughly equi-dimensional elements being considered here, the more general scaling corresponds to setting the spanwise length scale of the roughness equal to the local boundary-layer thickness, because it can be shown that this scaling includes the case where the spanwise length scale is large compared to the local boundary-layer thickness but small compared to the triple-deck scale. This would not be true for elongated roughness elements whose streamwise length scale is allowed to become large compared to their spanwise scale. But the present scaling also produces a more general far wake behaviour than the triple-deck scaling even in this case. We, therefore, write

$$y = y_r = \varepsilon h \tilde{F}(x, z), \tag{2.1}$$

$$u(x, y_r, z) = v(x, y_r, z) = w(x, y_r, z) = 0, \tag{2.2}$$

where all lengths are also normalized with respect to the boundary-layer thickness at $x^* = x_0^*$ unless otherwise noted, y_r is the roughness height, $\varepsilon \equiv R^{-1/6} = \delta^{1/3} \ll 1$, $x \equiv (x^* - x_0^*)/\delta^*$ and, as usual the fluid velocity

$$\boldsymbol{v} = \{u, v, w\} \tag{2.3}$$

is normalized by U_∞ and the pressure p by ρU_∞^2 where ρ is the fluid density.

3. Asymptotic structure of inner solution and governing equations

As will become clear subsequently, it is appropriate to divide the boundary-layer flow into an inner region in the vicinity of the roughness elements and an outer region that lies further downstream. The scaling in the former region is essentially the same as that used in Choudhari & Duck (1996). The solution in the main boundary layer,

where $y = O(1)$, should, therefore, expand as

$$\{u, v, w, p\} = \{U_0, \varepsilon^3 V_B, 0, 0\} + \varepsilon^2\{u_0, v_0, w_0, p_0\} + \varepsilon^3\{u_1, v_1, w_1, p_1\} + \cdots, \quad (3.1)$$

where

$$U_0 \equiv U_B(y) + \varepsilon^{7/4}\bar{U}_1(y) - \frac{y}{2}\varepsilon^3 x F''(y) \quad (3.2)$$

and

$$V_B(y) = \tfrac{1}{2}[yF'(y) - F(y)] \quad (3.3)$$

with $U_B(y) = F'(y)$ being the velocity determined from the usual Blasius equation in terms of the Blasius function $F(\eta_B)$ of the Blasius variable

$$\eta_B \equiv \frac{y^*}{x^*}\sqrt{x^* U_\infty / \nu^*} \quad (3.4)$$

with

$$U_B(\eta_B) = F'(\eta_B) \to \lambda\eta_B + O\left(\eta_B^4\right) \quad \text{as } \eta_B \to 0, \quad (3.5)$$

where $\lambda = 0.33206$ and $\varepsilon^{7/4}\bar{U}_1(y)$ is a small correction to the oncoming Blasius flow induced by the spanwise mean flow over the roughness, which was originally pointed out by Smith (1973) and is discussed more fully in Appendix A – it plays a purely passive role in the present problem and is included here only for the sake of completeness.

The zeroeth- and first-order solutions $\{u_i, v_i, w_i, p_i\}$, $(i = 0, 1)$ are functions of $\{x, y, z\}$ and are determined by

$$U_B(y)\frac{\partial u_i}{\partial x} + v_i U_B'(y) = -\frac{\partial p_i}{\partial x}, \quad (3.6)$$

$$U_B(y)\frac{\partial v_i}{\partial x} = -\frac{\partial p_i}{\partial y}, \quad (3.7)$$

$$U_B(y)\frac{\partial w_i}{\partial x} = -\frac{\partial p_i}{\partial z}, \quad (3.8)$$

$$\frac{\partial u_i}{\partial x} + \frac{\partial v_i}{\partial y} + \frac{\partial w_i}{\partial z} = 0, \quad (3.9)$$

subject to the boundary conditions

$$p_0(x, 0, z) = P(x, z),\ p_1(x, 0, z) = P^{(1)}(x, z);\ p_i(x, y, z) \to 0 \quad \text{as } y \to \infty, \quad (3.10)$$

where the zeroeth- and first-order wall pressures $P(x, z)$, $P^{(1)}(x, z)$ will be specified more precisely below.

Eliminating $\{u_j, v_j, w_j\}$ yields

$$\nabla^2 p_i - 2\frac{U_B'(y)}{U_B(y)}\frac{\partial p_i}{\partial y} = 0. \quad (3.11)$$

Since the roughness is assumed to be periodic in the spanwise direction and the flow in this region is linear, the spanwise and streamwise velocities posses the Fourier expansions

$$w_i(x, y, z) = -\frac{1}{U_B(y)}\sum_{n=-\infty}^{n=\infty}\int_{-\infty}^{\infty}\frac{n\tilde{P}_n^{(i)}(k)}{l\,k}\pi_n(y, k)\mathrm{e}^{\mathrm{i}(n\,z/l + kx)}\,\mathrm{d}k, \quad (3.12)$$

$$u_i(x,y,z) = -\frac{1}{U_B(y)}\sum_{n=-\infty}^{n=\infty}\int_{-\infty}^{\infty}\tilde{P}_n^{(i)}(k)\left[\frac{U_B'(y)}{k^2U_B(y)}\frac{\mathrm{d}\pi_n(y,k)}{\mathrm{d}y}+\pi_n(y,k)\right]\mathrm{e}^{\mathrm{i}(nz/l+kx)}\,\mathrm{d}k \tag{3.13}$$

in terms of the solution $\pi_n(y,k)$ to the unit boundary value problem

$$U_B^2(y)\frac{\mathrm{d}}{\mathrm{d}y}\left[\frac{1}{U_B^2(y)}\frac{\mathrm{d}\pi_n}{\mathrm{d}y}\right]-\left[\left(\frac{n}{l}\right)^2+k^2\right]\pi_n=0, n=0,\pm1,\pm2,\ldots, \tag{3.14}$$

$$\pi_n(0,k)=1, \pi_n(y,k)\to 0 \quad \text{as } y\to\infty, \tag{3.15}$$

where $\tilde{P}_n^{(0)}(k)$ and $\tilde{P}_n^{(1)}(k)$ are the streamwise wavenumber spanwise harmonic Fourier coefficients of the zeroeth and first wall pressures $P(x,z)$, $P^{(1)}(x,z)$, respectively. Since $y=0$ is a regular singular point of (3.14), it follows from (3.5) and the method of Frobenius that the two linearly independent solutions of (3.14) have Taylor series expansions about this point – a more explicit result for $n=k=0$ is given in Appendix A – and, therefore, that

$$\pi_n(y,k)\sim 1-\frac{1}{2}\left[\left(\frac{n}{l}\right)^2+k^2\right]y^2+\frac{1}{3!}\pi_n'''(0,k)y^3+O(y^4) \quad \text{as } y\to 0, \tag{3.16}$$

which shows that

$$w_i(x,y,z)\to -\frac{1}{\lambda y}\sum_{n=-\infty}^{n=\infty}\int_{-\infty}^{\infty}\frac{n\tilde{P}_n^{(i)}(k)}{l\,k}[1+O(y^2)]\mathrm{e}^{\mathrm{i}(nz/l+kx)}\,\mathrm{d}k, \tag{3.17}$$

and that

$$u_i(x,y,z)\to \frac{1}{\lambda\, y}\sum_{n=-\infty}^{n=\infty}\int_{-\infty}^{\infty}\frac{\tilde{P}_n^{(i)}(k)}{k^2}\left[\left(\frac{n}{l}\right)^2-\frac{1}{2}\pi_n'''(0,k)y\right]\mathrm{e}^{\mathrm{i}(nz/l+kx)}\,\mathrm{d}k, \quad \text{as } y\to 0. \tag{3.18}$$

The singularity in u_0 causes the expansion (3.1) to break down when

$$\breve{Y}\equiv y/\varepsilon = O(1), \tag{3.19}$$

and it is then necessary to obtain a new solution in this region, which we refer to here as the wall layer. Equations (3.17) and (3.18) show that the solution in this region must expand as (see Choudhari & Duck 1996)

$$\{u,v,w,p\}=\varepsilon\{U,\varepsilon\breve{V},W,\varepsilon P(x,z)\}+\varepsilon^2\left\{U^{(1)},\varepsilon\breve{V}^{(1)},W^{(1)},\varepsilon P^{(1)}(x,z)\right\}+\cdots, \tag{3.20}$$

where we have introduced the Prandtl transformation

$$Y\equiv y/\varepsilon - h\tilde{F}(x,z)=\breve{Y}-h\tilde{F}(x,z), \tag{3.21}$$

$$V\equiv \breve{V}-h(\tilde{F}_xU+\tilde{F}_zW), \tag{3.22}$$

$$V^{(1)}\equiv \breve{V}^{(1)}-h\left(\tilde{F}_xU^{(1)}+\tilde{F}_zW^{(1)}\right), \tag{3.23}$$

so that all velocity perturbations are functions of $\{x,Y,z\}$ and it is anticipated that the pressures do not vary across this thinner region to the required degree of approximation. Since the second term in the square brackets in (3.18) must match with an $O(\varepsilon^2)$ term in the wall layer, it is now clear why the $O(\varepsilon^3)$ term has to appear in the expansion (3.1). The leading order solution $\{U,V,W,P\}$ is determined from

the three-dimensional boundary-layer equations

$$U_x + V_Y + W_z = 0, \tag{3.24}$$

$$UW_x + VW_Y + WW_z = -P_z + W_{YY}, \tag{3.25}$$

$$UU_x + VU_Y + WU_z = -P_x + U_{YY}, \tag{3.26}$$

subject to the boundary conditions

$$U = V = W = 0, \quad \text{at } Y = 0, \tag{3.27}$$

$$U \to \lambda Y; V, W \to 0, \quad \text{as } x \to \pm\infty, \tag{3.28}$$

$$W_x \to -P_z/\lambda Y,\ U \to \lambda(Y + h\tilde{F}) + \frac{\breve{P}(x,z)}{\lambda Y} \quad \text{as } Y \to \infty, \tag{3.29}$$

where $\breve{P}(x,z)$ is determined by

$$\breve{P}(x,z) - P(x,z) \equiv \sum_{n=-\infty}^{n=\infty} \int_{-\infty}^{\infty} \frac{\tilde{P}_n^{(0)}(k)}{k^2} \left(\frac{n}{l}\right)^2 \mathrm{e}^{\mathrm{i}(nz/l+kx)}\,\mathrm{d}k, \tag{3.30}$$

or equivalently

$$\frac{\partial^2}{\partial x^2}\breve{P}(x,z) \equiv \left(\frac{\partial^2}{\partial z^2} + \frac{\partial^2}{\partial x^2}\right) P(x,z). \tag{3.31}$$

This system may be regarded as the three-dimensional analogue of the zero-displacement two-dimensional problem considered by Smith (1976*a*,*b*) even though there is a significant difference in its algebraic decay as $Y \to \infty$.

The next-order solution $\{U^{(1)}, V^{(1)}, W^{(1)}, P^{(1)}\}$ is determined from the linearized boundary-layer equations

$$U_x^{(1)} + V_Y^{(1)} + W_z^{(1)} = 0, \tag{3.32}$$

$$UU_x^{(1)} + VU_Y^{(1)} + WU_z^{(1)} + U^{(1)}U_x + V^{(1)}U_Y + W^{(1)}U_z = -P_x^{(1)} + U_{YY}^{(1)}, \tag{3.33}$$

$$UW_x^{(1)} + VW_Y^{(1)} + WW_z^{(1)} + U^{(1)}W_x + V^{(1)}W_Y + W^{(1)}W_z = -P_z^{(1)} + W_{YY}^{(1)}, \tag{3.34}$$

subject to the boundary conditions

$$W_x^{(1)} \to -P_z^{(1)}/\lambda Y,\ U_{xx}^{(1)} \to p_{0,yyy}(x,0,z)/2\lambda$$
$$= \frac{1}{2\lambda} \sum_{n=-\infty}^{n=\infty} \int_{-\infty}^{\infty} \tilde{P}_n^{(0)}(k)\pi_n'''(0,k)\,\mathrm{e}^{\mathrm{i}(nz/l+kx)}\,\mathrm{d}k \text{ as } Y \to \infty, \tag{3.35}$$

$$U^{(1)} = V^{(1)} = W^{(1)} = 0 \quad \text{at } Y = 0, \tag{3.36}$$

$$U^{(1)}, V^{(1)}, W^{(1)} \to 0 \quad \text{as } x \to \pm\infty. \tag{3.37}$$

Notice that the 1st order problem is just a linearized version of the zeroeth-order problem with the only difference being that the effective roughness height $\tilde{F}$ is replaced by the pressure term on the right side of (3.35), which is determined by the Rayleigh equation solution in the main boundary layer and (as we shall see) decays much more slowly than $\tilde{F}$ as $x \to \infty$. This is expected to cause the first-order solution to decay much more slowly than the zeroeth-order result.

4. Breakdown of inner solution

As in the linear case (see § 6) the wall pressures $P(x, z)$ and $P^{(1)}(x, z)$ are expected to decay algebraically as $x \to \infty$. (Smith 1973 proved that this is true in the two-dimensional zero displacement case, see also Smith *et al.* 1981.) However, the results of Appendix A show that the spanwise mean components $\bar{P}(x)$ and $\bar{P}^{(1)}(x)$ of $P(x, z)$ and $P^{(1)}(x, z)$, respectively behave differently from the spanwise variable component and must, therefore, be considered separately. We subtract out the mean components (which are of little interest in the present context because they do not contribute to the three-dimensional far wake flow that is being considered here) and require that $P(x, z) - \bar{P}(x)$ and $P^{(1)}(x, z) - \bar{P}^{(1)}(x)$ behave as $x^{-\alpha_0}$ and $x^{-\alpha_1}$ respectively for some real constants $\alpha_0, \alpha_1 > 0$ as $x \to \infty$. It then follows from (3.10) that

$$p_j(x, y, z) - \bar{p}_j(x, y) \sim \hat{p}_j(y, z)/x^{\alpha_j} \quad \text{as } x \to \infty, \tag{4.1}$$

where $\bar{p}_j(x, y)$ denotes the spanwise average component of $p_j(x, y, z)$ (and similarly for the remaining dependent variables $u_j(x, y, z)$, $v_j(x, y, z)$, $w_j(x, y, z)$).

The asymptotic formulas in Carrier, Krook & Pearson (1966, pp. 255–256) show that the corresponding Fourier coefficients $\tilde{P}_n^{(j)}(k) - \tilde{P}_0^{(j)}(k)$ must behave like

$$\tilde{P}_n^{(j)}(k) - \tilde{P}_0^{(j)}(k) \sim (\mathrm{i}k)^{\alpha_j - 1} \tilde{a}_n^{(j)} \quad \text{as } k \to 0, \tag{4.2}$$

where the $\tilde{a}_n^{(j)}$ are constants. The Carrier *et al.* (1966) formulas also show that the $\hat{p}_j(y, z)$ are related to the unit Rayleigh equation solutions π_n by

$$\hat{p}_j(y, z) \equiv -2 \sin \pi(\alpha_j - 1) \Gamma(\alpha_j) \sum_{\substack{n=-\infty \\ n \neq 0}}^{n=\infty} \pi_n(y, 0) \tilde{a}_n^{(j)} \mathrm{e}^{\mathrm{i}nz/l}. \tag{4.3}$$

The main-deck equations (3.6)–(3.8) then imply that

$$w_j(x, y, z) \sim \frac{1}{(\alpha_j - 1) x^{\alpha_j - 1}} \frac{1}{U_B(y)} \frac{\partial \hat{p}_j(y, z)}{\partial z}, \tag{4.4}$$

$$u_j(x, y, z) - \bar{u}_j(x, y) \sim \frac{1}{(\alpha_j - 1)(\alpha_j - 2) x^{\alpha_j - 2}} \frac{U_B'(y)}{U_B^2(y)} \frac{\partial}{\partial y} \hat{p}_j(y, z), \tag{4.5}$$

which shows that the zeroeth- and first-order kinetic energies will decay with respect to x when $\alpha_j > 2$ for both $j = 0$ and $j = 1$. Equations (3.16) and (4.3), therefore, imply that

$$\begin{aligned} \hat{p}_0(y, z) \sim & -2 \sin \pi(\alpha_0 - 1) \Gamma(\alpha_0) \\ & \times \sum_{\substack{n=-\infty \\ n \neq 0}}^{n=\infty} \left[1 - \frac{1}{2} \left(\frac{n}{l} \right)^2 y^2 + \frac{1}{3!} \pi_n'''(0, 0) y^3 + O(y^4) \right] \tilde{a}_n^{(0)} \mathrm{e}^{\mathrm{i}nz/l} \quad \text{as } y \to 0, \end{aligned} \tag{4.6}$$

and it then follows that

$$w_j(x, y, z) \sim \frac{1}{(\alpha_j - 1) x^{\alpha_0 - 1} \lambda} \frac{\partial \hat{p}_j(0, z)}{\partial z} \quad \text{as } y \to 0, \tag{4.7}$$

$$u_0(x, y, z) - \bar{u}_0(x, y) \sim \frac{1}{(\alpha_0 - 1)(\alpha_0 - 2) x^{\alpha_0 - 2} \lambda\, y} \left[\frac{\partial^2 \hat{p}_0(0, z)}{\partial z^2} + \frac{y}{2} \hat{p}_{0, y\, y\, y}(0, z) \right] \quad \text{as } y \to 0, \tag{4.8}$$

$$u_1(x, y, z) - \bar{u}_1(x, y) \sim \frac{1}{(\alpha_1 - 1)(\alpha_1 - 2) x^{\alpha_1 - 2} \lambda\, y} \frac{\partial^2 \hat{p}_1(0, z)}{\partial z^2} \quad \text{as } y \to 0, \tag{4.9}$$

where

$$\hat{p}_{0,y\,y\,y}(0,z) = -2\,\sin\pi(\alpha_0-1)\,\Gamma(\alpha_0)\sum_{\substack{n=-\infty\\ n\neq 0}}^{n=\infty}\pi_n'''(0,0)\tilde{a}_n^{(0)}\mathrm{e}^{\mathrm{i}nz/l}. \tag{4.10}$$

The wall layer solution is expected to decay relative to the Blasius velocity and, therefore, exhibit linear behaviour when $x \gg 1$ even when it is nonlinear in the vicinity of the roughness, which suggests that $\{U-\lambda Y, V, W, P\}$ should behave like a small perturbation of the original Blasius flow $U=\lambda Y$ and, therefore, satisfy the linear equations

$$\frac{\partial(U-\lambda Y)}{\partial x}+\frac{\mathrm{d}V}{\mathrm{d}Y}+\frac{\partial W}{\partial z}=0, \tag{4.11}$$

$$\lambda Y\frac{\partial(U-\lambda Y)}{\partial x}+\lambda V+\frac{\partial P}{\partial x}=\frac{\partial^2 U}{\partial Y^2}, \tag{4.12}$$

$$\lambda Y\frac{\partial W}{\partial x}+\frac{\partial P}{\partial z}=\frac{\partial^2 W}{\partial Y^2} \tag{4.13}$$

far downstream in the flow, whereas $\{U^{(1)}, V^{(1)}, W^{(1)}, P^{(1)}\}$ must satisfy

$$\frac{\partial U^{(1)}}{\partial x}+\frac{\mathrm{d}V^{(1)}}{\mathrm{d}Y}+\frac{\partial W^{(1)}}{\partial z}=0, \tag{4.14}$$

$$\lambda Y\frac{\partial U^{(1)}}{\partial x}+\lambda V^{(1)}+\frac{\partial P^{(1)}}{\partial x}=\frac{\partial^2 U^{(1)}}{\partial Y^2}, \tag{4.15}$$

$$\lambda Y\frac{\partial W^{(1)}}{\partial x}+\frac{\partial P^{(1)}}{\partial z}=\frac{\partial^2 W^{(1)}}{\partial Y^2} \tag{4.16}$$

there. The spanwise-mean and zero-spanwise-mean components can therefore be considered separately in the large x downstream region, which is important because the main boundary-layer solution shows that they behave differently at large x. The results for the spanwise-mean component are derived in Appendix A and only the spanwise-varying component (which is the one of principal interest) is dealt with here.

Since the corresponding zeroth- and first-order wall pressures $P(x,z)-\bar{P}(x)$ and $P^{(1)}(x,z)-\bar{P}^{(1)}(x)$ are assumed to decay like $x^{-\alpha_i}$ for $i=0,1$ as $x\to\infty$, and since (4.1)–(4.5) show that the spanwise variable pressure must decay out more rapidly than the streamwise velocity, these equations can be shown to possess similarity solutions of the form

$$W = x^{2/3-\alpha_0}\tilde{W}_0(\eta,z), \quad W^{(1)} = x^{2/3-\alpha_1}\tilde{W}_1(\eta,z), \tag{4.17}$$

$$U-\bar{U} = x^{5/3-\alpha_0}\tilde{U}_0(\eta,z), \quad U^{(1)}-\overline{U^{(1)}} = x^{5/3-\alpha_1}\tilde{U}_1(\eta,z) \tag{4.18}$$

and

$$V-\bar{V} = x^{1-\alpha_0}\lambda^{-1/3}\tilde{V}_0(\eta,z),\ V^{(1)}-\overline{V^{(1)}} = x^{1-\alpha_1}\lambda^{-1/3}\tilde{V}_1(\eta,z), \tag{4.19}$$

where

$$\eta \equiv \lambda^{1/3}Y/x^{1/3}, \tag{4.20}$$

and $\tilde{U}_j, \tilde{V}_j, \tilde{W}_j$ satisfy

$$-\left[\frac{\eta}{3}\frac{\partial\tilde{U}_j}{\partial\eta}+\left(\alpha_j-\frac{5}{3}\right)\tilde{U}_j\right]+\frac{\partial\tilde{V}_j}{\partial\eta}+\frac{\partial\tilde{W}_j}{\partial z}=0, \tag{4.21}$$

$$\frac{\partial^2 \tilde{U}_j}{\partial \eta^2} + \eta \left[\frac{\eta}{3} \frac{\partial \tilde{U}_j}{\partial \eta} + \left(\alpha_j - \frac{5}{3} \right) \tilde{U}_j \right] = \tilde{V}_j, \tag{4.22}$$

$$\frac{\partial^2 \tilde{W}_j}{\partial \eta^2} + \eta \left[\frac{\eta}{3} \frac{\partial \tilde{W}_j}{\partial \eta} + \left(\alpha_j - \frac{2}{3} \right) \tilde{W}_j \right] = \lambda^{-2/3} \frac{\partial}{\partial z} \hat{p}_j(0, z), \tag{4.23}$$

subject to the boundary conditions

$$\tilde{U}_j(0, z) = \tilde{V}_j(0, z) = \tilde{W}_j(0, z) = 0. \tag{4.24}$$

Equations (3.1), (3.20)–(3.23), (4.7)–(4.9) and (4.17)–(4.20) show that these solutions will match onto the main boundary-layer solution if we set

$$\alpha_1 = \alpha_0 - 1/3, \tag{4.25}$$

and require that

$$\tilde{W}_j(\eta, z) \to \frac{1}{(\alpha_j - 1)\lambda^{2/3}\eta} \frac{\partial \hat{p}_j(0, z)}{\partial z}, \tag{4.26}$$

$$\tilde{U}_0(\eta, z) \to \frac{1}{(\alpha_0 - 1)(\alpha_0 - 2)\lambda^{2/3}\eta} \frac{\partial^2 \hat{p}_0(0, z)}{\partial z^2} \tag{4.27}$$

and

$$\tilde{U}_1(\eta, z) \to \frac{\hat{p}_{0,yyy}(0, z)}{(\alpha_0 - 1)(\alpha_0 - 2)\, 2\lambda} + \frac{1}{(\alpha_1 - 1)(\alpha_1 - 2)\, \lambda^{2/3}\eta} \frac{\partial^2 \hat{p}_1(0, z)}{\partial z^2}, \tag{4.28}$$

as $\eta \to \infty$, where $\hat{p}_{0,yyy}(0, z)$ is given by (4.10).

Eliminating $\tilde{V}_j$ from (4.21) and (4.22) yields

$$\frac{\partial^3 \tilde{U}_j}{\partial \eta^3} + \frac{\eta}{3} \left[\eta \frac{\partial^2 \tilde{U}_j}{\partial \eta^2} + (3\alpha_0 - 4 - j) \frac{\partial \tilde{U}_j}{\partial \eta} \right] + \tilde{W}_{j,z} = 0, \tag{4.29}$$

where $\tilde{U}_j$ must satisfy

$$\frac{\partial^2 \tilde{U}_j}{\partial \eta^2} = 0 \quad \text{at } \eta = 0. \tag{4.30}$$

So setting

$$\hat{W}_j = -\left[\frac{\eta}{3} \frac{\partial \hat{U}_j}{\partial \eta} + \left(\alpha_0 - \frac{5 + j}{3} \right) \hat{U}_j \right], \tag{4.31}$$

where

$$\frac{\partial^2 \hat{U}_j}{\partial \eta^2} + \eta \left[\frac{\eta}{3} \frac{\partial \hat{U}_j}{\partial \eta} + \left(\alpha_0 - \frac{5 + j}{3} \right) \hat{U}_j \right] = C_j, \tag{4.32}$$

or equivalently

$$\frac{\partial^2 \hat{U}_j}{\partial \eta^2} - \eta \hat{W}_j = C_j, \tag{4.33}$$

implies that

$$\frac{\partial \hat{W}_j}{\partial \eta} = -\frac{\eta}{3} \frac{\partial^2 \hat{U}_j}{\partial \eta^2} - \left(\alpha_0 - \frac{4 + j}{3} \right) \frac{\partial \hat{U}_j}{\partial \eta}, \quad \frac{\partial^2 \hat{W}_j}{\partial \eta^2} = -\frac{\eta}{3} \frac{\partial^3 \hat{U}_j}{\partial \eta^3} - \left(\alpha_0 - 1 - \frac{j}{3} \right) \frac{\partial^2 \hat{U}_j}{\partial \eta^2}, \tag{4.34}$$

and therefore

$$\frac{\partial^2 \hat{W}_j}{\partial \eta^2} + \eta \left[\frac{\eta}{3} \frac{\partial \hat{W}_j}{\partial \eta} + \left(\alpha_0 - \frac{2+j}{3} \right) \hat{W}_j \right] = - \left(\alpha_0 - 1 - \frac{j}{3} \right) C_j. \tag{4.35}$$

Then since

$$\frac{\partial^3 \hat{U}_j}{\partial \eta^3} + \frac{\eta}{3} \left[\eta \frac{\partial^2 \hat{U}_j}{\partial \eta^2} + (3\alpha_0 - 4 - j) \frac{\partial \hat{U}_j}{\partial \eta} \right]$$
$$= \frac{\partial}{\partial \eta} \left\{ \frac{\partial^2 \hat{U}_j}{\partial \eta^2} + \frac{\eta}{3} \left[\eta \frac{\partial \hat{U}_j}{\partial \eta} + (3\alpha_0 - 4 - j) \hat{U}_j \right] \right\} - \frac{2}{3} \eta \frac{\partial \hat{U}_j}{\partial \eta} - \frac{1}{3} (3\alpha_0 - 4 - j) \hat{U}_j, \tag{4.36}$$

$\hat{U}_j$ must satisfy

$$\frac{\partial^3 \hat{U}_j}{\partial \eta^3} + \frac{\eta}{3} \left[\eta \frac{\partial^2 \hat{U}_j}{\partial \eta^2} + (3\alpha_0 - 4 - j) \frac{\partial \hat{U}_j}{\partial \eta} \right] - \hat{W}_j = 0. \tag{4.37}$$

It therefore follows that $\tilde{W}_j$ will satisfy (4.23) together with the boundary conditions (4.24) and (4.26) if we require that

$$\hat{U}_j(0) = 0 \quad \text{and} \quad \hat{U}_j(\eta) \sim \eta^{-1} \quad \text{as } \eta \to \infty, \tag{4.38}$$

and set

$$\tilde{W}_j = \frac{-1}{\lambda^{2/3} \left(\alpha_0 - 1 - \frac{j}{3} \right) C_j} \frac{\partial \hat{p}_j(0, z)}{\partial z} \hat{W}_j(\eta). \tag{4.39}$$

Then

$$\tilde{U}_j = \frac{1}{\lambda^{2/3} \left(\alpha_0 - 1 - \frac{j}{3} \right) C_j} \frac{\partial^2 \hat{p}_j(0, z)}{\partial z^2} \hat{U}_j(\eta) \tag{4.40}$$

will be a particular solution of (4.29) that satisfies the boundary conditions (4.24) and (4.27). However this solution will not in general satisfy the boundary conditions (4.30) and (4.28) and an appropriate homogeneous solution of (4.29), say $\tilde{U}_{H,j}$, must be added to the result in order to satisfy these additional conditions. The homogeneous solution $\tilde{U}_{H,j}$ must vanish at $\eta = 0$ for $j = 0, 1$ while $\tilde{U}_{H,0}$ must be of $O(\eta^{-1})$ at infinity and $\tilde{U}_{H,1}$ must asymptote to a non-zero constant there.

Introducing the new independent variable

$$\varsigma = -\eta^3/9, \tag{4.41}$$

shows that $\tilde{U}_{j,\eta}$ satisfies the inhomogeneous confluent hypergeometric equation

$$\varsigma \frac{\partial^2 \tilde{U}_{j,\eta}}{\partial \varsigma^2} + \left(\frac{2}{3} - \varsigma \right) \frac{\partial \tilde{U}_{j,\eta}}{\partial \varsigma} - \frac{3\alpha_0 - 4 - j}{3} \tilde{U}_{j,\eta} = \frac{1}{\eta} \tilde{W}_{j,z}, \tag{4.42}$$

which posses the homogeneous solution (Abramowitz & Stegun 1965, pp. 504ff.)

$$\tilde{U}_{Hj} \equiv \tilde{B}_{Hj} \int_0^\eta {}_1F_1 \left(\frac{3\alpha_0 - 4 - j}{3}, \frac{2}{3}; -\frac{\eta^3}{9} \right) \mathrm{d}\eta + \tilde{C}_{Hj} \int_0^\eta \eta {}_1F_1 \left(\frac{3\alpha_0 - 3 - j}{3}, \frac{4}{3}; -\frac{\eta^3}{9} \right) \mathrm{d}\eta. \tag{4.43}$$

But (4.32) and (4.33) can also possess homogeneous solutions, say $\hat{U}_{H,j}$, $\hat{W}_{H,j}$, that vanishes at $\eta = 0$ and remain bounded but do not vanish as $\eta \to \infty$. The most general

solution is then obtained by putting

$$\tilde{U}_j \Rightarrow \frac{1}{\lambda^{2/3}\left(\alpha_0 - 1 - \frac{j}{3}\right) C_j} \frac{\partial^2 \hat{p}_j(0,z)}{\partial z^2} [\hat{U}_j(\eta) + \hat{C}_{Hj} \hat{U}_{H,j}(\eta)] + \tilde{U}_{H,j}, \tag{4.44}$$

and the boundary condition (4.30) will be satisfied if $\tilde{C}_{Hj}$ can be chosen such that

$$\tilde{C}_{Hj} = \frac{-1}{\lambda^{2/3}\left(\alpha_0 - 1 - \frac{j}{3}\right) C_j} \frac{\partial^2 \hat{p}_j(0,z)}{\partial z^2} \hat{U}_j''(0) = \frac{-1}{\lambda^{2/3}\left(\alpha_0 - 1 - \frac{j}{3}\right)} \frac{\partial^2 \hat{p}_j(0,z)}{\partial z^2}. \tag{4.45}$$

Inserting the independent variable (4.41) into (4.32) shows that $\hat{U}_{H,j}$ must satisfy the hypergeometric equation

$$\varsigma \frac{\partial^2 \hat{U}_{H,j}}{\partial \varsigma^2} + \left(\frac{2}{3} - \varsigma\right) \frac{\partial \hat{U}_{H,j}}{\partial \varsigma} - \frac{3\alpha_0 - 5 - j}{3} \hat{U}_{H,j} = 0, \tag{4.46}$$

and it therefore follows that

$$\hat{U}_{H,j} = \eta_1 F_1\left(\frac{3\alpha_0 - 4 - j}{3}, \frac{4}{3}; -\frac{\eta^3}{9}\right). \tag{4.47}$$

Each of the integrals in (4.43) will converge when $\alpha_0 > (5 + j)/3$ and $\tilde{B}_{Hj}$ can then be chosen so that $\tilde{U}_{H0}(\eta)$ is proportional to $\eta^{-(3\alpha_0 - 5 - j)}$ as $\eta \to \infty$, since

$$F_1\left(\frac{3\alpha_0 - 4 - j}{3}, \frac{2}{3}; -\frac{\eta^3}{9}\right) \tag{4.48}$$

and

$$\eta_1 F_1\left(\frac{3\alpha_0 - 3 - j}{3}, \frac{4}{3}; -\frac{\eta^3}{9}\right) \tag{4.49}$$

both decay like $\eta^{-(3\alpha_0 - 4 - j)}$ as $\eta \to \infty$. And since

$$\eta_1 F_1\left(\frac{3\alpha_0 - 4 - j}{3}, \frac{4}{3}; -\frac{\eta^3}{9}\right) \sim \eta^{-(3\alpha_0 - 5 - j)} \quad \text{as } \eta \to \infty, \tag{4.50}$$

$\hat{C}_{H,j}$ can then be chosen so that

$$\tilde{U}_j \to \frac{1}{\lambda^{2/3}\left(\alpha_0 - 1 - \frac{j}{3}\right) C_j} \frac{\partial^2 \hat{p}_j(0,z)}{\partial z^2} \hat{U}_j(\eta) \quad \text{as } \eta \to \infty, \tag{4.51}$$

and the boundary condition (4.27) will then be satisfied.

However the combined integral in (4.43) will converge even when $\alpha_0 \leqslant (5 + j)/3$ if $\tilde{B}_{Hj}$ is set equal to

$$\tilde{B}_{Hj} = -\frac{\Gamma(2 - \alpha_0 + j/3)\Gamma(1/3)\tilde{C}_{Hj}}{\Gamma(2 - \alpha_0 + (j+1)/3)\Gamma(2/3)3^{1/3}}, \tag{4.52}$$

because (see (13.1.9) in Abramowitz & Stegun 1965, p. 504) the integrand will then be proportional to $e^{-\eta^3/9} U((6 + j - 3\alpha_0)/3, 2/3, \eta^3/9)$ (where $U(a, b, z)$ denotes the Hypergeometric equation solution defined by (13.1.3) of Abramowitz & Stegun 1965) and, therefore, vanishes exponentially fast as $\eta \to \infty$. It will be proportional to $e^{-\eta^3/9}$ when $\alpha_0 = (6 + j)/3$.

It follows that $\hat{C}_{H,0}$ can be chosen so that (4.48) is satisfied when $\alpha_0 = 5/3$ and, therefore, that the boundary condition (4.27) can also satisfied in this case. The

homogeneous solution $\hat{U}_{H,0}$ will then be given by

$$\hat{U}_{H0} = \int_0^\eta \exp\left(-\frac{\eta^3}{9}\right) \mathrm{d}\eta, \tag{4.53}$$

and the integrand in (4.43) will become

$$\tilde{U}_{H0} = -\frac{\tilde{C}_{H0}[\Gamma(1/3)]^2\sqrt{3}}{2\pi 3^{1/3}} \int_0^\eta \mathrm{e}^{-\eta^3/9} U(1/3, 2/3, \eta^3/9)\, \mathrm{d}\eta. \tag{4.54}$$

Equation (4.18) shows that $U - \bar{U}$ will then approach a constant value as $x \to \infty$ at fixed η and z, i.e. it will not decay as $x \to \infty$ at fixed η, but the linearization (4.11)–(4.13) will still be valid because the scaled Blasius velocity $U_B/\varepsilon \approx \lambda Y = \lambda^{2/3} x^{1/3} \eta$ increases like $x^{1/3}$ as $x \to \infty$ at fixed η. However, this is the smallest value of α_0 for which the linearization will be valid, because matching the wall layer and main-deck solutions requires that $\alpha_0 = n/3$ for $n = 1, 2, \ldots$ (since the inner expansion of the latter can only involve integral powers of y) and $U - \bar{U}$ will be proportional to $x^{1/3}$ as $x \to \infty$ at fixed η when α_0 is equal to $4/3$.

When $\alpha_0 > 2$ (i.e. when u_0 decays in the streamwise direction), $\tilde{B}_{H0}$ can always be chosen so that

$$\tilde{U}_{H0}(\eta) = o(\eta^{-1}) \quad \text{as } \eta \to \infty. \tag{4.55}$$

The lower bound for α_0 therefore appears to be $7/3$ in this case since, as noted above, matching with the outer solution requires that $\alpha_0 . = n/3$ for $n = 1, 2, \ldots$. The constant $\hat{C}_{H,0}$ is then arbitrary and can be determined by matching with the upstream solution.

When $\alpha_0 > 7/3$, $\hat{C}_{H1}$ can be set to zero in (4.44) and the boundary condition (4.28) can be satisfied for any combination of $\hat{p}_{1zz}(0, z)$ and $\hat{p}_{0,yyy}(0, z)$ by choosing $\tilde{B}_{H1}$ so that

$$\int_0^\infty \left[\tilde{B}_{H\,1} {}_1F_1\left(\frac{3\alpha_0 - 5}{3}, \frac{2}{3}; -\frac{\eta^3}{9}\right) + \tilde{C}_{H\,1}\eta_1 F_1\left(\frac{3\alpha_0 - 4}{3}, \frac{4}{3}; -\frac{\eta^3}{9}\right)\right] \mathrm{d}\eta = \frac{\hat{p}_{0,yyy}(0, z)}{(\alpha_0 - 1)(\alpha_0 - 2)\, 2\lambda}, \tag{4.56}$$

since the integrals will converge in this case.

5. Outer solution

Equations (4.5) and (4.25) show that the magnitude $\varepsilon(u_1 - \bar{u}_1)$ of the first-order streamwise velocity perturbation will be equal to that of the zeroeth-order streamwise velocity perturbation $u_0 - \bar{u}_0$ and cause the expansion (3.1) to breakdown when $\varepsilon x^{1/3} = (\delta x)^{1/3} = O(1)$. It is, therefore, necessary to obtain a new expansion in the 'outer region' where

$$X \equiv x^*/x_0^* = \delta x + 1 \tag{5.1}$$

is $O(1)$, which must then be of the form

$$\{u, v, w, p\} = \{U_B(\eta_B), \delta V_B(X, \eta_B), 0, 0\} + \varepsilon^3\{\bar{\tilde{u}}(X, y), \delta\bar{\tilde{v}}(X, y), 0, \bar{\tilde{p}}(X, y)\} + \cdots + \varepsilon^{3\alpha-4}\{\tilde{u}(X, y, z), \delta\tilde{v}(X, y, z), \delta\tilde{w}(X, y, z), \delta^2\tilde{p}(X, y, z)\} + \cdots, \tag{5.2}$$

where the spanwise-mean component has been separated out from the zero-spanwise-mean component because of the difference in their orders of magnitude. The spanwise

variable perturbations $\{\tilde{u}, \tilde{v}, \tilde{w}, \tilde{p}\}$ are determined from the LBR equations

$$\tilde{u}_X + \tilde{v}_y + \tilde{w}_z = 0, \tag{5.3}$$

$$U_B\tilde{u}_X + V_B\tilde{u}_y + \tilde{u}U_{B,X} + \tilde{v}U_{B,y} = \tilde{u}_{yy} + \tilde{u}_{zz}, \tag{5.4}$$

$$U_B\tilde{v}_X + V_B\,\tilde{v}_y + \tilde{u}\,V_{B,X} + \tilde{v}\,V_{B,y} = -\tilde{p}_y + \tilde{v}_{yy} + \tilde{v}_{zz}, \tag{5.5}$$

$$U_B\tilde{w}_X + V_B\tilde{w}_y = -\tilde{p}_z + \tilde{w}_{yy} + \tilde{w}_{zz}, \tag{5.6}$$

subject to the transverse boundary conditions

$$\tilde{u}, \tilde{v}, \tilde{w} = 0; \text{ for } y = 0; \ \tilde{u}, \tilde{v}, \tilde{w}, \tilde{p} \to 0 \quad \text{as } y \to \infty, \tag{5.7}$$

and appropriate upstream matching conditions. The spanwise mean solution $\overline{\tilde{u}(X, y)}$, $\delta\overline{\tilde{v}(X, y)}$ is determined from the two-dimensional constant pressure linearized boundary-layer equations (see (A 25)).

5.1. *Main boundary layer*

When $X \to 1$ and $y = O(1)$, (5.3)–(5.6) possess a power series solution of the form

$$\tilde{u} = \frac{1}{(X-1)^{\alpha-2}}\sum_{k=0}^{\infty}(X-1)^k\tilde{u}_k^{(0)}(y,z) + \frac{1}{(X-1)^{\alpha-7/3}}\sum_{k=0}^{\infty}(X-1)^k\tilde{u}_k^{(1)}(y,z), \tag{5.8}$$

$$\begin{Bmatrix}\tilde{v}\\ \tilde{w}\end{Bmatrix} = \frac{1}{(X-1)^{\alpha-1}}\sum_{k=0}^{\infty}(X-1)^k\begin{Bmatrix}\tilde{v}_k^{(0)}(y,z)\\ \tilde{w}_k^{(0)}(y,z)\end{Bmatrix} + \frac{1}{(X-1)^{\alpha-4/3}}\sum_{k=0}^{\infty}(X-1)^k\begin{Bmatrix}\tilde{v}_k^{(1)}(y,z)\\ \tilde{w}_k^{(1)}(y,z)\end{Bmatrix}, \tag{5.9}$$

$$\tilde{p} = \frac{1}{(X-1)^{\alpha}}\sum_{k=0}^{\infty}(X-1)^k\tilde{p}_k^{(0)}(y,z) + \frac{1}{(X-1)^{\alpha-1/3}}\sum_{k=0}^{\infty}(X-1)^k\tilde{p}_k^{(1)}(y,z), \tag{5.10}$$

where $\tilde{u}_0^{(j)}$, $\tilde{v}_0^{(j)}$, $\tilde{w}_0^{(j)}$, $\tilde{p}_0^{(j)}$ satisfy

$$\left(2-\alpha+\frac{j}{3}\right)\tilde{u}_0^{(j)} + \tilde{v}_{0,y}^{(j)} + \tilde{w}_{0,z}^{(j)} = 0, \tag{5.11}$$

$$\left(2-\alpha+\frac{j}{3}\right)U_B(y)\tilde{u}_0^{(j)} + \tilde{v}_0^{(j)}U_B'(y) = 0, \tag{5.12}$$

$$\left(1-\alpha+\frac{j}{3}\right)U_B(y)\begin{Bmatrix}\tilde{v}_0^{(j)}\\ \tilde{w}_0^{(j)}\end{Bmatrix} = -\begin{Bmatrix}\tilde{p}_{0,y}^{(j)}\\ \tilde{p}_{0,z}^{(j)}\end{Bmatrix}, \tag{5.13}$$

and $\tilde{u}_1^{(j)}$, $\tilde{v}_1^{(j)}$, $\tilde{w}_1^{(j)}$, $\tilde{p}_1^{(j)}$ satisfy the equations given in Appendix B. The inner expansion of the outer solution as $X \to 1$ is therefore

$$\begin{aligned}\varepsilon^{3\alpha-4}\tilde{u} \sim{}& \frac{\varepsilon^{3\alpha-4}}{(X-1)^{\alpha-2}}\left[\tilde{u}_0^{(0)}(y,z) + (X-1)\tilde{u}_1^{(0)}(y,z) + \cdots\right]\\ &+\frac{\varepsilon^{3\alpha-4}}{(X-1)^{\alpha-7/3}}[\tilde{u}_0^{(1)}(y,z) + (X-1)\tilde{u}_1^{(1)}(y,z) + \cdots]\\ ={}& \varepsilon^2\left[\frac{\tilde{u}_0^{(0)}(y,z)}{x^{\alpha-2}} + \delta x^{1-\alpha}\tilde{u}_1^{(0)}(y,z) + \cdots\right] + \varepsilon^3\left[\frac{\tilde{u}_0^{(1)}(y,z)}{x^{\alpha-7/3}} + \delta x^{4/3-\alpha}\tilde{u}_1^{(1)}(y,z) + \cdots\right],\end{aligned} \tag{5.14}$$

$$\delta\varepsilon^{3\alpha-4}\begin{Bmatrix}\tilde{v}\\ \tilde{w}\end{Bmatrix}\sim\frac{\delta\varepsilon^{3\alpha-4}}{(X-1)^{\alpha-1}}\left[\begin{Bmatrix}\tilde{v}_0^{(0)}(y,z)\\ \tilde{w}_0^{(0)}(y,z)\end{Bmatrix}+(X-1)\begin{Bmatrix}\tilde{v}_1^{(0)}(y,z)\\ \tilde{w}_1^{(0)}(y,z)\end{Bmatrix}+\cdots\right]$$
$$+\frac{\delta\varepsilon^{3\alpha-4}}{(X-1)^{\alpha-4/3}}\left[\begin{Bmatrix}\tilde{v}_0^{(1)}(y,z)\\ \tilde{w}_0^{(1)}(y,z)\end{Bmatrix}+(X-1)\begin{Bmatrix}\tilde{v}_1^{(1)}(y,z)\\ \tilde{w}_1^{(1)}(y,z)\end{Bmatrix}+\cdots\right]$$
$$=\varepsilon^2\left[\frac{1}{x^{\alpha-1}}\begin{Bmatrix}\tilde{v}_0^{(0)}(y,z)\\ \tilde{w}_0^{(0)}(y,z)\end{Bmatrix}+\delta x^{2-\alpha}\begin{Bmatrix}\tilde{v}_1^{(0)}(y,z)\\ \tilde{w}_1^{(0)}(y,z)\end{Bmatrix}+\cdots\right]$$
$$+\varepsilon^3\left[\frac{\tilde{v}_0^{(1)}(y,z)}{x^{\alpha-4/3}}\begin{Bmatrix}\tilde{v}_0^{(1)}(y,z)\\ \tilde{w}_0^{(0)}(y,z)\end{Bmatrix}+\delta x^{7/3-\alpha}\begin{Bmatrix}\tilde{v}_1^{(1)}(y,z)\\ \tilde{w}_1^{(1)}(y,z)\end{Bmatrix}+\cdots\right], \quad (5.15)$$

$$\varepsilon^{3\alpha-4}\delta^2\,\tilde{p}\sim\frac{\varepsilon^{3\alpha-4}\delta^2}{(X-1)^{\alpha}}\left[\tilde{p}_0^{(0)}(y,z)+(X-1)\tilde{p}_1^{(0)}(y,z)+\cdots\right]$$
$$+\frac{\varepsilon^{3\alpha-4}\delta^2}{(X-1)^{\alpha-1/3}}\left[\tilde{p}_0^{(1)}(y,z)+(X-1)\tilde{p}_1^{(1)}(y,z)+\cdots\right]$$
$$=\varepsilon^2\left[\frac{\tilde{p}_0^{(0)}(y,z)}{x^{\alpha}}+\frac{\delta}{x^{\alpha-1}}\tilde{p}_1^{(0)}(y,z)+\cdots\right]+\varepsilon^3\left[\frac{\tilde{p}_0^{(1)}(y,z)}{x^{\alpha-1/3}}+\frac{\delta}{x^{\alpha-4/3}}\tilde{p}_1^{(1)}(y,z)+\cdots\right]. \quad (5.16)$$

Eliminating $\tilde{u}_0^{(0)}$, $\tilde{v}_0^{(0)}$, $\tilde{w}_0^{(0)}$ implies that $\tilde{p}_0^{(j)}$ satisfies

$$\frac{\partial^2\tilde{p}_0^{(j)}}{\partial y^2}+\frac{\partial^2\tilde{p}_0^{(j)}}{\partial z^2}-2\frac{U_B'}{U_B}\frac{\partial\tilde{p}_0^{(j)}}{\partial y}=0, \quad (5.17)$$

but

$$U_B^2\frac{\mathrm{d}}{\mathrm{d}y}\left[\frac{1}{U_B^2}\frac{\mathrm{d}\pi_n(y,0)}{\mathrm{d}y}\right]-\left(\frac{n}{l}\right)^2\pi_n(y,0)=0 \quad (5.18)$$

implies that $\hat{p}_j$ satisfies

$$\frac{\partial^2\hat{p}_j}{\partial y^2}+\frac{\partial^2\hat{p}_j}{\partial z^2}-2\frac{U_B'}{U_B}\frac{\partial\hat{p}_j}{\partial y}=0. \quad (5.19)$$

Then since $\tilde{p}_0^{(j)}(y,z)$ and $\hat{p}_j(y,z)$ both satisfy the same equation, it follows from (4.25) that the inner and outer solutions will only match if we set

$$\alpha=\alpha_0, \quad (5.20)$$

$$\tilde{p}_0^{(0)}(y,z)=\hat{p}_0(y,z), \quad (5.21)$$

and

$$\tilde{p}_0^{(1)}(y,z)=\hat{p}_1(y,z). \quad (5.22)$$

Equations (5.8)–(5.10) suggest that $\tilde{u}$ will begin to increasing when $(X-1)>\tilde{u}_0^{(0)}(y,z)/\tilde{u}_1^{(0)}(y,z)$. But this solution does not satisfy the correct wall boundary condition since (3.15), (4.3), (5.13) and (5.21) show that $\tilde{w}_0^{(0)}\to\infty$ as $y\to 0$. In fact it follows from the method of Frobenius that

$$p_0^{(j)}\sim p_0^{(j)}(0,z)+\frac{y^2}{2}\frac{\partial^2}{\partial z^2}p_0^{(j)}(0,z)+\frac{y^3}{3!}\left(\frac{\partial^3 p_0^{(j)}}{\partial y^3}\right)_{y=0} \quad (5.23)$$

when $\tilde{p}_0^{(0)}(0, z)$ is non-zero, which implies that

$$\tilde{w}_0^{(j)} \sim \frac{1}{\left(\alpha - 1 - \frac{j}{3}\right)\lambda y} \frac{\partial p_0^{(j)}(0, z)}{\partial z}, \tag{5.24}$$

$$\tilde{v}_0^{(j)} \sim \frac{1}{\left(\alpha - 1 - \frac{j}{3}\right)\lambda} \frac{\partial^2}{\partial z^2} p_0^{(j)}(0, z) + \frac{y}{2\left(\alpha - 1 - \frac{j}{3}\right)\lambda} \left(\frac{\partial^3 p_0^{(j)}}{\partial y^3}\right)_{y=0}, \tag{5.25}$$

$$\tilde{u}_0^{(j)} \sim \frac{1}{\left(\alpha - 2 - \frac{j}{3}\right)\left(\alpha - 1 - \frac{j}{3}\right) y\lambda} \frac{\partial^2}{\partial z^2} p_0^{(j)}(0, z) + \frac{1}{2\left(\alpha - 2 - \frac{j}{3}\right)\left(\alpha - 1 - \frac{j}{3}\right)\lambda} \left(\frac{\partial^3 p_0^{(j)}}{\partial y^3}\right)_{y=0}. \tag{5.26}$$

This breakdown occurs because the lowest order terms in the expansion (5.8)–(5.10) satisfy inviscid equations and, therefore, cannot satisfy the viscous wall boundary conditions. This means that it is necessary to derive new solutions in a viscous wall layer at the surface of the plate.

5.2. *Wall layer*

These solutions must satisfy the linearized boundary-layer equations (4.11)–(4.16) whose viscous and inertial terms will be of the same order of magnitude when

$$y/X \sim 1/y^2, \tag{5.27}$$

which suggests introducing the similarity variable (4.20)

$$\eta = \frac{\lambda^{1/3} y}{(X-1)^{1/3}} \tag{5.28}$$

rewritten in terms of the outer variables. It follows from the spanwise momentum equation (5.6) and the expansion (5.10) that these terms will balance with the spanwise pressure gradient if $\tilde{w}$ is of the form

$$\tilde{w} = (X-1)^{2/3-\alpha} \left[\tilde{W}_0(\eta, z) + (X-1)^{1/3}\, \tilde{W}_1(\eta, z)\right] \tag{5.29}$$

while continuity and the streamwise momentum equation (5.4) then imply that $\tilde{u}$ and $\tilde{v}$ must be of the form

$$\tilde{u} = (X-1)^{5/3-\alpha}[\tilde{U}_0(\eta, z) + (X-1)^{1/3}\tilde{U}_1(\eta, z)] \tag{5.30}$$

and

$$\tilde{v} = (X-1)^{1-\alpha}\lambda^{-1/3}[\tilde{V}_0(\eta, z) + (X-1)^{1/3}\tilde{V}_1(\eta, z)]. \tag{5.31}$$

Inserting these into the LBR equations (5.3)–(5.6) shows that $\tilde{U}_j, \tilde{V}_j, \tilde{W}_j$ must satisfy (4.21)–(4.23) with α_1 and α_0 given by (4.25) and (5.20) subject to the boundary condition (4.24). However, matching with (5.24)–(5.26) implies that $\tilde{U}_j, \tilde{W}_j$ must also satisfy conditions (4.26)–(4.28) and therefore that the (outer) wall layer solution is identical to the asymptotic wall layer of §4–in fact it is merely the continuation of that layer into the outer region. This shows that there is an overlap domain in which the asymptotic form of the inner solution matches onto the outer LBR equation solution that satisfies (5.8)–(5.10) as $X \to 1$.

6. Linear solution

The 'outer' far wake flow is completely determined by the induced (inner solution) wall pressures in the general nonlinear solution constructed in the previous sections. But this solution must be found numerically. The present section considers the $h \ll 1$ linearized solution in order to fix the inner wall pressure decay rate $\alpha = \alpha_0$ and explicitly relate these pressures to the roughness geometry.

6.1. *The inner solution*

When $h \ll 1$, the leading order wall layer solution and its first-order correction posses the expansions

$$\{U, V, W, P(x,z)\} = \{\lambda Y, 0.0, 0\} + h\{U_1^{(0)}, V_1^{(0)}, W_1^{(0)}, P_1^{(0)}(x,z)\} + h^2\{U_2^{(0)}, V_2^{(0)}, W_2^{(0)}, P_2^{(0)}(x,z)\} + \cdots, \quad (6.1)$$

and

$$\{U^{(1)}, V^{(1)}, W^{(1)}, P^{(1)}\} = h\{U_1^{(1)}, V_1^{(1)}, W_1^{(1)}, P_1^{(1)}\} + \cdots, \quad (6.2)$$

where $\{U_1^{(j)}, V_1^{(j)}, W_1^{(j)}, P_1^{(j)}\}$ satisfy the linear equations (4.11)–(4.16) together with the boundary conditions (3.27) and (3.36) and the matching conditions (3.29) and (3.35).

Equations (3.27) and (3.36) then imply that

$$\widehat{U}_n^{(i)} = \widehat{W}_n^{(i)} = \widehat{V}_n^{(i)} = 0, \text{ at } Y = 0, \quad (6.3)$$

while (3.29) and (3.35) imply that

$$\widehat{U}_n^{(0)} = \lambda \widehat{F}_n(k) + O(Y^{-1}), \ \widehat{W}_n^{(0)} = O(Y^{-1}) \quad \text{as } Y \to \infty, \quad (6.4)$$

and

$$\widehat{U}_n^{(1)}(k) \to -\frac{\pi_n'''(0,k)}{2\lambda k^2}\tilde{P}_n^{(0)}, \ \widehat{W}_1^{(1)} = O(Y^{-1}) \quad \text{as } Y \to \infty, \quad (6.5)$$

where $\{\widehat{U}_n^{(i)}(Y,k), \widehat{V}_n^{(i)}(Y,k), \widehat{W}_n^{(i)}(Y,k), \widehat{P}_n^{(i)}(k), \widehat{F}_n(k)\}$ is defined by

$$\{U_1^{(i)}, V_1^{(i)}, W_1^{(i)}, P_1^{(i)}(x,z), \tilde{F}(x,z)\} = \sum_{n=-\infty}^{n=\infty} \int_{-\infty}^{\infty} \{\widehat{U}_n^{(i)}(Y,k), \widehat{V}_n^{(i)}(Y,k), \widehat{W}_n^{(i)}(Y,k), \widehat{P}_n^{(i)}(k), \widehat{F}_n(k)\} e^{i(nz/l+kx)}\, dk, \quad (6.6)$$

and it follows from the linearized boundary-layer equations (4.11)–(4.16) that

$$ik\widehat{U}_n^{(i)} + \frac{d\widehat{V}_n^{(i)}}{dY} + i\left(\frac{n}{l}\right)\widehat{W}_n^{(i)} = 0, \quad (6.7)$$

$$ik\lambda Y\widehat{U}_n^{(i)} + \lambda\widehat{V}_n^{(i)} + ik\widehat{P}_n^{(i)} = \frac{d^2\widehat{U}_n^{(i)}}{dY^2}, \quad (6.8)$$

$$ik\lambda Y\widehat{W}_n^{(i)} + i\left(\frac{n}{l}\right)\widehat{P}_n^{(i)} = \frac{d^2\widehat{W}_n^{(i)}}{dY^2} \quad (6.9)$$

for $i = 0, 1$ and, therefore, that

$$ik\lambda Y\frac{d\widehat{U}_n^{(i)}}{dY} - i\left(\frac{n}{l}\right)\lambda\widehat{W}_n^{(i)} = \frac{d^3\widehat{U}_n^{(i)}}{dY^3}, \quad (6.10)$$

$$\frac{\mathrm{d}^2\hat{U}_n^{(i)}}{\mathrm{d}Y^2} = ik\hat{P}_n^{(i)} \quad \text{for } Y = 0, \quad i = 0, 1, \tag{6.11}$$

$$\hat{P}_n^{(i)} = \tilde{P}_n^{(i)}, \tag{6.12}$$

$$\hat{W}_n^{(i)} = -\frac{in\pi}{(ik\lambda)^{2/3}\, l}\tilde{P}_n^{(i)}(k)\left[Gi(\bar{\eta}) - \frac{1}{\sqrt{3}}Ai(\bar{\eta})\right], \tag{6.13}$$

$$\hat{U}_n^{(i)} = -\frac{\lambda\pi\tilde{P}_n^{(i)}(k)}{(ik\lambda)^{5/3}}\left\{\left(\frac{n}{l}\right)^2\left[Gi(\bar{\eta}) - \frac{1}{\sqrt{3}}Ai(\bar{\eta})\right] - \Gamma\left(\frac{1}{3}\right)\frac{3^{1/3}}{\pi}\left[\left(\frac{n}{l}\right)^2 + k^2\right]\int_0^{\bar{\eta}} Ai(\tilde{\eta})\,\mathrm{d}\tilde{\eta}\right\} \tag{6.14}$$

and

$$\lambda\hat{V}_n^{(i)}(k) = -ik\lambda Y\hat{U}_n^{(i)}(k) - ik\hat{P}_n^{(i)} + \frac{\mathrm{d}^2\hat{U}_n^{(i)}(k)}{\mathrm{d}Y^2} \tag{6.15}$$

for $i = 0, 1$, where

$$\bar{\eta} \equiv (ik\lambda)^{1/3}\, Y, \tag{6.16}$$

and the Ai and Gi denote the Airy functions defined in Abramowitz & Stegun (1964, pp. 446, 448). Then since

$$Gi(\bar{\eta}) \sim \frac{1}{\pi\bar{\eta}} = \frac{1}{\pi(ik\lambda)^{1/3}Y} \quad \text{as } Y \to \infty \tag{6.17}$$

it follows from (6.4), (6.5) and (6.14) that

$$\tilde{P}_n^{(0)}(k) = \frac{(ik\lambda)^{5/3}9^{1/3}}{[(n/l)^2 + k^2]\Gamma(1/3)}\hat{F}_n(k), \tag{6.18}$$

$$\tilde{P}_n^{(1)}(k) = \frac{\pi_n'''(0,k)9^{1/3}\tilde{P}_n^{(0)}(k)}{2[(n/l)^2 + k^2]\Gamma(1/3)(ik\lambda)^{1/3}} = \frac{(ik\lambda)^{4/3}9^{2/3}\pi_n'''(0,k)}{2\{[(n/l)^2 + k^2]\Gamma(1/3)\}^2}\hat{F}_n(k), \tag{6.19}$$

$$\hat{W}_n^{(0)}(k) \sim -\frac{i\,n\,9^{1/3}(ik\lambda)^{2/3}}{Y\,l[(n/l)^2 + k^2]\;\Gamma(1/3)}\hat{F}_n(k), \tag{6.20}$$

and

$$\hat{U}_n^{(0)}(k) - \lambda\hat{F}_n(k) \sim -\frac{\lambda(9)^{1/3}(n/l)^2}{\Gamma(1/3)[(n/l)^2 + k^2]}\frac{\hat{F}_n(k)}{(ik\lambda)^{1/3}Y}, \tag{6.21}$$

as $Y \to \infty$.

We now require that $\tilde{F}(x, z) = O(x^{-1})$ as $x \to \infty$ and, consequently, that $\bar{F}_n(k)$ will remain bounded (and, in general, non-zero) at $k = 0$. It then follows from (6.18) and (6.19) that

$$\alpha = \alpha_0 = 8/3, \tag{6.22}$$

which means that the coefficients in (4.3) are now given by

$$\tilde{a}_n^{(0)} = \frac{2hl^2\lambda^{5/3}9^{1/3}}{n^2\Gamma(1/3)}\hat{F}_n(0), \tag{6.23}$$

$$\tilde{a}_n^{(1)} = \frac{h\lambda^{4/3}l^4 9^{2/3}\pi_n'''(0,0)}{n^4\Gamma(1/3)^2}\hat{F}_n(0). \tag{6.24}$$

Equations (6.6), (6.13) and (6.18) imply that

$$W_1^{(0)} = \frac{\pi 9^{1/3}}{\Gamma(1/3)} \sum_{n=-\infty}^{n=\infty} \int_{-\infty}^{\infty} \widehat{F}_n(k) \frac{n\lambda k}{l[(n/l)^2 + k^2]} \left[Gi(\bar{\eta}) - \frac{1}{\sqrt{3}} Ai(\bar{\eta}) \right] \mathrm{e}^{\mathrm{i}(nz/l + kx)} \, \mathrm{d}k, \quad (6.25)$$

$$W_1^{(1)} = \frac{-\pi 9^{2/3}}{2[\Gamma(1/3)]^2} \sum_{n=-\infty}^{n=\infty} \int_{-\infty}^{\infty} \frac{in\pi_n'''(0,k)\widehat{F}_n(k)(ik\lambda)^{2/3}}{l[(n/l)^2 + k^2]^2} \left[Gi(\bar{\eta}) - \frac{1}{\sqrt{3}} Ai(\bar{\eta}) \right] \mathrm{e}^{\mathrm{i}(nz/l + kx)} \, \mathrm{d}k, \quad (6.26)$$

and consequently that

$$W_1^{(0)} = \frac{\pi 9^{1/3}}{x^2 \Gamma(1/3)} \sum_{n=-\infty}^{n=\infty} \int_{-\infty}^{\infty} \widehat{F}_n \left(\frac{\kappa}{x} \right) \frac{n\lambda\kappa}{l(n^2/l^2 + \kappa^2/x^2)} \left[Gi((i\kappa)^{1/3}\eta) - \frac{1}{\sqrt{3}} Ai((i\kappa)^{1/3}\eta) \right]$$
$$\times \mathrm{e}^{\mathrm{i}(nz/l + \kappa)} \, \mathrm{d}\kappa \to \frac{\pi \lambda^{5/3} 9^{1/3}}{x^2 \lambda^{2/3} \Gamma(1/3)} \left[\sum_{\substack{n=-\infty \\ n \neq 0}}^{n=\infty} \frac{l \widehat{F}_n(0)}{in} e^{inz/l} \right] \hat{W}_{p0}(\eta) \quad \text{as } x \to \infty \text{ with } \eta = O(1) \quad (6.27)$$

and

$$W_1^{(1)} = \frac{-\pi 9^{2/3}}{x^{5/3} 2[\Gamma(1/3)]^2} \times \sum_{n=-\infty}^{n=\infty} \int_{-\infty}^{\infty} \pi_n''' \left(0, \frac{\kappa}{x} \right) \widehat{F}_n \left(\frac{\kappa}{x} \right) \frac{in(i\kappa\lambda)^{2/3}}{l(n^2/l^2 + \kappa^2/x^2)^2}$$
$$\times \left[Gi((i\kappa)^{1/3}\eta) - \frac{1}{\sqrt{3}} Ai((i\kappa)^{1/3}\eta) \right] e^{i(nz/l + \kappa)} \, \mathrm{d}\kappa \to \frac{-\pi i \, (9\lambda)^{2/3}}{x^{5/3} 2\lambda^{2/3} [\Gamma(1/3)]^2}$$
$$\times \sum_{\substack{n=-\infty \\ n \neq 0}}^{n=\infty} \left[\pi_n'''(0,0) \frac{l^3 \widehat{F}_n(0)}{n^3} e^{inz/l} \right] \hat{W}_{p1}(\eta) \quad \text{as } x \to \infty \text{ with } \eta = O(1), \quad (6.28)$$

where η is defined by (4.20) and finally

$$\hat{W}_{pj}(\eta) \equiv \int_{-\infty}^{\infty} (\kappa i)^{1-j/3} \left[Gi((i\kappa)^{1/3}\eta) - \frac{1}{\sqrt{3}} Ai((i\kappa)^{1/3}\eta) \right] \mathrm{e}^{\mathrm{i}\kappa} \, \mathrm{d}\kappa$$
$$= +\text{exponentially small terms (as } x \to \infty) \quad (6.29)$$
$$\oint_C (\kappa i)^{1-j/3} \left[Gi((i\kappa)^{1/3}\eta) - \frac{1}{\sqrt{3}} Ai((i\kappa)^{1/3}\eta) \right] \mathrm{e}^{i\kappa} \mathrm{d}\kappa$$

for $j = 0, 1$. The Fourier transformed roughness shape function $\widehat{F}_n(k)$ is assumed to be analytic in the upper half-plane (i.e. the roughness height is assumed to be identically zero for $x > 0$) so that the contour C can be taken as shown in figure 2.

Equations (6.27) and (6.28) are clearly consistent with (4.17) and (4.25).

6.2. *The outer solution*

Since, as noted in § 5, matching with the inner solution requires that $\tilde{p}_0^{(j)}(y, z) = \hat{p}_j(y, z)$, it follows from (4.2)–(4.3), (6.23) and (6.24) that

$$\tilde{p}_0^{(0)}(y, z) = \hat{p}_0(y, z) = \frac{10\sqrt{3}\Gamma(2/3)}{9\Gamma(1/3)} 9^{1/3} \lambda^{5/3} h \sum_{\substack{n=-\infty \\ n \neq 0}}^{n=\infty} \pi_n(y, 0) \frac{l^2 \widehat{F}_n(0)}{n^2} \mathrm{e}^{\mathrm{i}nz/l}, \quad (6.30)$$

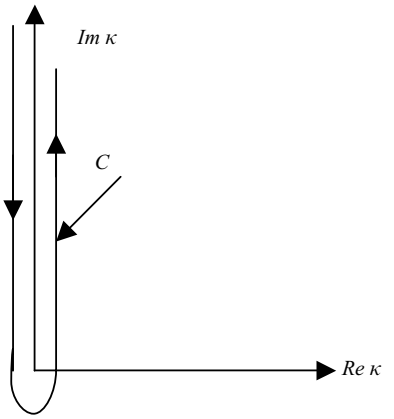

FIGURE 2. Deformation of inversion contour.

and

$$\tilde{p}_0^{(1)}(y,z) = \hat{p}_1(y,z) = \frac{2\sqrt{3}\,9^{2/3}\lambda^{4/3}}{9\Gamma(1/3)} h \sum_{\substack{n=-\infty \\ n\neq 0}}^{n=\infty} \pi_n(y,0) \frac{l^4 \widehat{F}_n(0)\pi_n'''(0,0)}{n^4} \mathrm{e}^{\mathrm{i}nz/l}. \tag{6.31}$$

But (6.22) implies that (4.43) becomes

$$\tilde{U}_{H\,j,\eta} = \tilde{B}_{H\,j1} F_1\left(\frac{4-j}{3}, \frac{2}{3}; -\frac{\eta^3}{9}\right) + \tilde{C}_{Hj}\eta_1 F_1\left(\frac{2-j}{3}+1, 1+\frac{1}{3}; -\frac{\eta^3}{9}\right) \quad \text{for } j = 0, 1. \tag{6.32}$$

And since (by (13.4.10) in Abramowitz & Stegun 1965, p. 507)

$$\eta_1 F_1\left(\frac{4}{3}, \frac{2}{3}; -\frac{\eta^3}{9}\right) = \frac{\partial}{\partial\eta}\eta_1 F_1\left(\frac{1}{3}, \frac{2}{3}; -\frac{\eta^3}{9}\right), \tag{6.33}$$

$$\eta_1 F_1\left(\frac{2}{3}+1\,, 1+\frac{1}{3}; -\frac{\eta^3}{9}\right) = \frac{1}{2}\frac{\partial}{\partial\eta}\eta^2{}_1 F_1\left(\frac{2}{3}, 1+\frac{1}{3}; -\frac{\eta^3}{9}\right) \tag{6.34}$$

it follows that

$$\tilde{U}_{H0} = \eta\left[\tilde{B}_{H01} F_1\left(\frac{1}{3}, \frac{2}{3}; -\frac{\eta^3}{9}\right) + \tilde{C}_{H0}\frac{1}{2}\eta_1 F_1\left(\frac{2}{3}, 1+\frac{1}{3}; -\frac{\eta^3}{9}\right)\right]. \tag{6.35}$$

Equation (4.52) requires that (by (13.1.5) in Abramowitz & Stegun 1965, p. 504)

$$\tilde{B}_{H\,0} = -\left[\frac{\Gamma(1/3)}{\Gamma(2/3)}\right]^2 \frac{\tilde{C}_{H0}}{(23)^{1/3}}, \tag{6.36}$$

and, therefore, (by (13.1.9) in Abramowitz & Stegun, 1965)

$$\tilde{U}_{H0} = -\frac{\eta\sqrt{3}\,\tilde{C}_{H0}\,[\Gamma(1/3)]^2}{3^{1/3}4\pi}\mathrm{e}^{-\eta^3/9} U\left(\frac{1}{3}, \frac{2}{3}, \frac{\eta^3}{9}\right), \tag{6.37}$$

which shows that $\tilde{U}_{H,0}$ actually decays exponentially fast as $\eta \to \infty$.

Equation (4.32) now possesses the homogeneous solution

$$\hat{U}_{1\,j} = \eta^{(1-j)} e^{-\eta^3/9}, \tag{6.38}$$

and it therefore follows from the method of variation of parameters that the solutions to (4.32) that satisfy the required boundary condition (4.38) are given by

$$\hat{U}_0 = \frac{C_0}{2}\eta e^{-\eta^3/9}\left[\int_0^\eta e^{\tilde{\eta}^3/9}\,d\tilde{\eta} + \hat{C}_0\right], \tag{6.39}$$

$$\hat{U}_1 = C_1\left[e^{-\eta^3/9}\int_0^\eta \tilde{\eta}e^{\tilde{\eta}^3/9}\,d\tilde{\eta} + \hat{C}_1 e^{-\eta^3/9}\int_0^\eta e^{\tilde{\eta}^3/9}\,d\tilde{\eta}\right], \tag{6.40}$$

where $\hat{C}_j$ are arbitrary constants.

The hypergeometric function in the second term on the left side of (4.53) becomes

$$\eta_1 F_1\left(\frac{4}{3},\frac{4}{3};-\frac{\eta^3}{9}\right) = e^{-\eta^3/9}, \tag{6.41}$$

when $\alpha_0 = 8/3$. And since

$$\int_0^\infty \eta e^{-\eta^3/9}\,d\eta = \frac{9^{2/3}}{3}\int_0^\infty t^{-1/3}e^{-t}\,dt = \frac{9^{2/3}}{3}\Gamma(2/3) \tag{6.42}$$

it follows from (6.30) and (6.31) that

$$\tilde{B}_{H,1} = 0, \tag{6.43}$$

and, therefore, that $\tilde{C}_{H,j}$ is given by (4.45). Then since

$$\frac{d^2Ai((i\kappa)^{1/3}\eta)}{d\eta^2} = i\kappa\eta Ai((i\kappa)^{1/3}\eta),\ \frac{\eta^2}{3}\frac{dAi((i\kappa)^{1/3}\eta)}{d\eta} = \eta\kappa\frac{dAi((i\kappa)^{1/3}\eta)}{d\kappa},$$
$$\frac{d^2Gi((i\kappa)^{1/3}\eta)}{d\eta^2} = i\kappa\eta Gi((i\kappa)^{1/3}\eta) - \frac{(i\kappa)^{2/3}}{\pi}, \tag{6.44}$$

the function (6.29) satisfies (4.35) with

$$C_j = \frac{\sqrt{3}}{\pi}\Gamma\left(\frac{5-j}{3}\right), \tag{6.45}$$

and the function

$$\hat{U}_{pj}(\eta) \equiv \oint_C (\kappa i)^{-j/3}\left[Gi\left((i\kappa)^{1/3}\eta\right) - \frac{1}{\sqrt{3}}Ai\left((i\kappa)^{1/3}\eta\right)\right]e^{i\kappa}d\kappa \tag{6.46}$$

satisfies equations (4.31) and (4.32) with $\hat{W}_j = \hat{W}_{pj}$. It, therefore, follows that $\hat{W}_{pj}$ and $\hat{U}_{pj}$ are given by (6.39) and (6.40) and that

$$\hat{U}'_{p0}(0) = \frac{\sqrt{3}}{2\pi}\Gamma\left(\frac{5}{3}\right)\hat{C}_0 = \left[Gi'(0) - \frac{1}{\sqrt{3}}Ai'(0)\right]\oint_C (\kappa i)^{1-j/3}e^{i\kappa}d\kappa$$
$$= -\left[Gi'(0) - \frac{1}{\sqrt{3}}Ai'(0)\right]\sqrt{3}\,\Gamma(4/3) = -\frac{2\Gamma(4/3)\sqrt{3}}{\sqrt{3}3^{1/3}\Gamma(1/3)} = -\frac{2}{3^{1/3}3} \tag{6.47}$$

or

$$\hat{C}_0 = -\frac{4\pi}{3^{1/3}3\sqrt{3}\Gamma\left(\frac{5}{3}\right)} = -\frac{2\pi}{3^{1/3}\sqrt{3}\,\Gamma\left(\frac{2}{3}\right)} \tag{6.48}$$

and

$$\hat{U}'_{p1}(0) = \frac{\sqrt{3}}{\pi}\Gamma\left(\frac{4}{3}\right)\hat{C}_1 = \left[Gi'(0) - \frac{1}{\sqrt{3}}Ai(0)\right]\oint_C e^{i\kappa}d\kappa = 0 \tag{6.49}$$

or

$$\hat{C}_1 = 0. \tag{6.50}$$

It now follows that

$$\hat{W}_j = -\frac{1}{\pi 3\sqrt{3}}\eta\left\{\left[2(2-j)-\frac{\eta^3}{3}\right]\mathrm{e}^{-\eta^3/9}\left[\Gamma\left(\frac{2-j}{3}\right)\eta^{-j}\int_0^\eta \tilde{\eta}^j \mathrm{e}^{\tilde{\eta}^3/9}\,\mathrm{d}\tilde{\eta} - \delta_{j,0}\frac{2\pi}{\sqrt{3}3^{1/3}}\right]\right.$$
$$\left. + \Gamma\left(\frac{2-j}{3}\right)\eta\right\}. \tag{6.51}$$

7. Numerical procedures

7.1. *The outer linear boundary region problem for the linear inner solution*

A finite-difference approach on a staggered grid (Harlow & Welch 1965) was used to solve the LBR equations (5.3)–(5.6) in order to avoid the decoupling between pressure and velocities. Periodic boundary conditions were imposed in the spanwise direction. The numerical method is similar to the one used in Leib *et al.* (1999) with a grid-convergence approach similar to that used in Goldstein & Sescu (2008). The pressure variable $\pi_n(y, 0)$ in (4.3) was found by using a second-order finite difference scheme, which requires a tri-diagonal matrix inversion by the Thomas algorithm (Tannehill, Anderson & Pletcher 1997, Appendix A), to solve (5.18) subject to the boundary conditions $\pi_n(0, 0) = 1$ and $\pi_n(y, 0) \to 0$ as $y \to \infty$.

The relevant LBR equation solutions must satisfy the initial or upstream matching conditions given in Appendix C, with the zeroeth- and first-order pressure variables now given explicitly by (6.30) and (6.31). The confluent hypergeometric function $\eta_1 F_1(a, b; z)$ was computed by using (13.1.2) of Abramowitz & Stegun (1965, p. 504) for small $|z|$, and the asymptotic expansion (13.5.1) (Abramowitz & Stegun 1965, p. 508) for large $|z|$ with the two curves being matched with spline functions whenever necessary. Simpson's rule was used for the numerical integrations that appear in these results.

7.2. *The inner nonlinear problem*

An iterative scheme based on that of Smith (1991) was used to solve the full (nonlinear) problem (3.24)–(3.29). (This was also the methodology used in Choudhari & Duck 1996.) Differentiating the x-momentum equation (3.26) with respect to x, and the z-momentum equation (3.25) with respect to z, and adding the results leads to the equation

$$U\frac{\partial U^*}{\partial x} + V^*\frac{\partial U}{\partial Y} = -E^* + \frac{\partial^2 U^*}{\partial Y^2} - S(x, Y, z), \tag{7.1}$$

where

$$U^* = \frac{\partial U}{\partial x} + \frac{\partial W}{\partial z}, \tag{7.2}$$

$$V^* = \frac{\partial V}{\partial x}, \tag{7.3}$$

$$E^*(x, z) = \frac{\partial^2 P}{\partial x^2} + \frac{\partial^2 P}{\partial z^2}, \tag{7.4}$$

$$S(x, Y, z) = \left(\frac{\partial U}{\partial x}\right)^2 + V\frac{\partial^2 U}{\partial x \partial Y} + 2\left(\frac{\partial W}{\partial x}\right)\left(\frac{\partial U}{\partial z}\right) + W\frac{\partial^2 U}{\partial x \partial z} + \frac{\partial}{\partial z}\left(V\frac{\partial W}{\partial Y} + W\frac{\partial W}{\partial z}\right). \tag{7.5}$$

The continuity equation (differentiated with respect to x) becomes

$$\frac{\partial U^*}{\partial x} + \frac{\partial V^*}{\partial Y} = 0. \tag{7.6}$$

The resulting system, in particular (7.1) and (7.2), may be regarded as quasi-two-dimensional, and, therefore, suggests introducing the quasi-stream function Ψ^*

$$U^* = \Psi^*_Y,\ V^* = -\Psi^*_x \tag{7.7}$$

in order to satisfy (7.6). The resulting problem was then solved iteratively by approximating the z-momentum equation, continuity and (7.1) using a combination of Crank–Nicolson differencing (in x) and second-order central differencing in both Y and z. Having estimated U, V and W(starting with an initial guess), the finite difference approximation to (7.1) was then solved (in a standard x-wise marching manner), in conjunction with (7.6), to yield estimates for Ψ^*, U^*, V^* and $E^*(x, z)$. (An analogous procedure could be used for the two-dimensional problem of Smith 1976*a*,*b*) Next the Poisson's equation (7.4) for the pressure was approximated by second-order central differences, with symmetry/antisymmetry conditions at the two extremes of z, Dirichlet conditions at the upstream extremum of x and Neumann conditions at the downstream extremum of x; the resulting system (using the values of $E^*(x, z)$ evaluated in the previous step) was then solved in a direct manner, exploiting the sparseness properties of the system. Next the finite-difference approximation to the z-momentum equation was solved (in a marching manner, not dissimilar from that used on (7.1)), to determine W, utilizing the pressure values obtained in the preceding step; finally U and V were simply deduced from (7.2) and (7.3). The entire procedure was then repeated, until sufficient convergence was achieved. This procedure was also used to obtain numerical solutions to the 'linear' ($h \ll 1$) problem.

8. Results and discussion

This paper considers the wakes behind an array of roughness elements with spanwise wavenumber $\beta^* = 1/(l\, x_0^* \delta)$. The focus being on the far wake region where the spanwise mean component of the flow is governed by the two-dimensional zero pressure gradient linearized boundary-layer equations and the spanwise variable component is governed by the LBR equations (5.3)–(5.6). Then since the deviation $\{\tilde{\bar{u}}(X, y), \delta\tilde{\bar{v}}(X, y), 0\}$ of the spanwise mean velocity vector from the Blasius flow must decay out very quickly on the long streamwise length scale X, the main emphasis is on the spanwise variable component $\{\tilde{u}, \delta\tilde{v}, \delta\tilde{w}, \delta^2\tilde{p}\}$.

We have shown that the spanwise variable pressure decays like $x^{-\alpha}$ when the short streamwise length scale x becomes large and that $\alpha = 8/3$ in the linear case, although the analysis of §4 clearly shows that α can be as small as $5/3$ in the general nonlinear case. But an $x^{-\alpha}\ln(x)$ decay rate is also possible since the wake equations (4.11)–(4.13) have an asymptotic solution of this form which we ignore for now. It, therefore, follows from (5.2) that the (normalized) spanwise variable component of the streamwise velocity perturbation $\varepsilon^{3\alpha-4}\tilde{u}$ will be proportional to $U_\infty R^{-1/6}$ when α takes on its minimum value and, as can be seen from (5.11) to (5.13)

and from (6.30) to $h\varepsilon^4$ in the linear case. But it follows from (2.1) that h is essentially equal to $k/\varepsilon\delta^* = k/\varepsilon^4 x_0^*$, where k denotes the dimensional roughness height in the usual notation. So the (normalized) spanwise variable component of the streamwise velocity perturbation will then be proportional to k/x_0^* independent of Reynolds number.

The relevant solutions to the LBR equations (5.3)–(5.6) must satisfy the upstream matching conditions (5.14)–(5.16) in the main boundary layer where $y = O(1)$ and match onto the solution (5.29)–(5.31) in the wall layer where $\eta = O(1)$. The upstream matching can be implemented by first forming a uniformly valid 'composite' solution for the two regions and then matching the LBR solutions with the result, which is written out in Appendix C.

Since the outer solution is determined from linear equations it is appropriate to divide it into its spanwise Fourier components with the nth component, say $\varepsilon^{3\alpha-4}\{\tilde{U}_n, \delta\tilde{V}_n, \delta\tilde{W}_n, \delta^2\tilde{P}_n\}$, determined by

$$\varepsilon^{3\alpha-4}\{\tilde{u}, \delta\tilde{v}, \delta\tilde{w}, \delta^2\tilde{p}\} = \varepsilon^{3\alpha-4}\sum_{\substack{n=-\infty \\ n\neq 0}}^{\infty} \mathrm{e}^{\mathrm{i}nz/l}\{\tilde{U}_n, \delta\tilde{V}_n, \delta\tilde{W}_n, \delta^2\tilde{P}_n\}. \tag{8.1}$$

These components will be completely independent when the inner solution is linear, but will be coupled through the upstream boundary conditions when it is not. However, it makes sense to consider the scaled modal energy components

$$E_n(X) \equiv \int_0^\infty \left[|\tilde{U}_n(X, y)|^2 + \delta^2|\tilde{V}_n(X, y)|^2 + \delta^2|\tilde{W}_n(X, y)|^2\right] \mathrm{d}y \tag{8.2}$$

of the profile averaged kinetic energy

$$\mathscr{E}(X) \equiv \delta(\varepsilon^{3\alpha-4})^2 \int_0^\infty \left[|\tilde{u}(X, y)|^2 + \delta^2|\tilde{v}(X, y)|^2 + \delta^2|\tilde{w}(X, y)|^2\right] \mathrm{d}y, \tag{8.3}$$

even when the inner solution is nonlinear. But most of the computations were carried out for the linear case, where the modal energies are completely independent. The linear solution has the additional advantage of greatly simplifying the treatment of multiple roughness rows since the solutions for each individual row can be superposed and the inner streamwise length scale of the roughness elements is asymptotically negligible compared to the streamwise length scale on which the far wakes evolve. The linear far wake solution for identical rows of roughness elements can, therefore, be found by simply multiplying the single row solution by the number of rows.

8.1. *The linear problem*

Specific results were obtained for two different roughness shape functions: the sharply discontinuous but very compact function

$$\tilde{F}(x, z) = \begin{cases} 1, & 0 \leqslant |z - \pi l| \leqslant d/2, \\ 0, & \text{otherwise}, \end{cases} \tag{8.4}$$

used by Choudhari & Fischer (2005) to model the experimental configuration of White & Ergin (2003) and referred to here as Case 1 and the very smooth but less localized function

$$\tilde{F}(x, z) = \exp\{-[x^2 + (z - \pi l)^2]/d^2\}, \tag{8.5}$$

referred to here as Case 2.

	Energy growth factors		Energy decay from maximum energy over $x =$ (1.5,16) to $x = 16$	
Roughness parameters	Case 1	Case 2	Case 1	Case 2
$l = 5$ and $d/l = 2.76$	246	246	1.62	1.62
$l = 10$ and $d/l = 1.38$	753	753	1.00	1.00
$l = 5$ and $d/l = 1.38$	246	246	1.62	1.62

TABLE 1. Energy growth factors

Equations (5.11)–(5.13), (6.30) and (8.1) show that nth spanwise Fourier component $\varepsilon^{3\alpha-4}\{\tilde{U}_n, \delta\tilde{V}_n, \delta\tilde{W}_n, \delta^2\tilde{P}_n\}$ of $\varepsilon^{3\alpha-4}\{\tilde{u}, \delta\tilde{v}, \delta\tilde{w}, \delta^2\tilde{p}\}$ will be proportional to $\widehat{F}_n(0)$ where

$$\widehat{F}_n(0) = \frac{(-1)^n l}{2\pi D^2}\int_0^1 J_0(nDx)x\,\mathrm{d}x, \tag{8.6}$$

in Case 1 and

$$\widehat{F}_n(0) = \frac{lD^2}{\pi}\mathrm{e}^{-(nD)^2-in\pi}Re\,erf(\pi/2D + inD), \tag{8.7}$$

in Case 2 where

$$D \equiv d/2l, \tag{8.8}$$

which suggests that $\varepsilon^{3\alpha-4}\tilde{u}$ will actually be proportional to $k/\delta x_0^*$ for fixed l^*/x_0^*. But since k/x_0^* is proportional to $\sqrt{\delta^3 Re_k}$, where Re_k denotes the Reynolds number based on roughness height and the boundary-layer velocity at this height, $\varepsilon^{3\alpha-4}\tilde{u}$ should be proportional to $\sqrt{Re_k}/R^{1/4}$. The profile averaged energy (8.3), which is approximately equal to

$$\mathscr{E}_0 \equiv \delta\int_0^\infty |\varepsilon^{3\alpha-4}\tilde{u}(X, y)|^2\,\mathrm{d}y \tag{8.9}$$

when $X - 1$ is sufficiently large, should, then be proportional to Re_k.

Figure 3 is a plot of the scaled modal energy components (8.2) of the profile averaged energy (8.3) for Cases 1 and 2 with various values of l and D. We have put $\delta = 0$ because the crossflow terms only contribute at very small values of the Reynolds number R when $X - 1$ is sufficiently large. The figure shows that there is a sharp minimum in the modal energies between $X = 1.1$ and $X = 1.5$, which can be interpreted as the initiation point for the transient energy growth over a finite interval downstream of this location. The maximum modal energy appears to be an increasing function of the array wavelength relative to the boundary-layer thickness at the roughness location, $l = l^*/\delta^*$ for roughness elements with fixed plan form size. Notice that the energy drops off very quickly with increasing harmonic index n in both cases. There seems to be very little difference between the two cases with the main difference occurring at the larger d/l value, where the final amplitude is significantly larger in Case 2 – presumably because the wake interference effects are larger.

Table 1 shows the growth factors associated with the increase in modal energy $E_1(x)$ of the fundamental harmonic from the minimum energy location in figures 3(a) and 3(b) up to its maximum within the downstream region. Notice that the value of the growth factor is nearly independent of the geometry of the roughness element (either shape or planform size), being primarily determined by the array spacing parameter l.

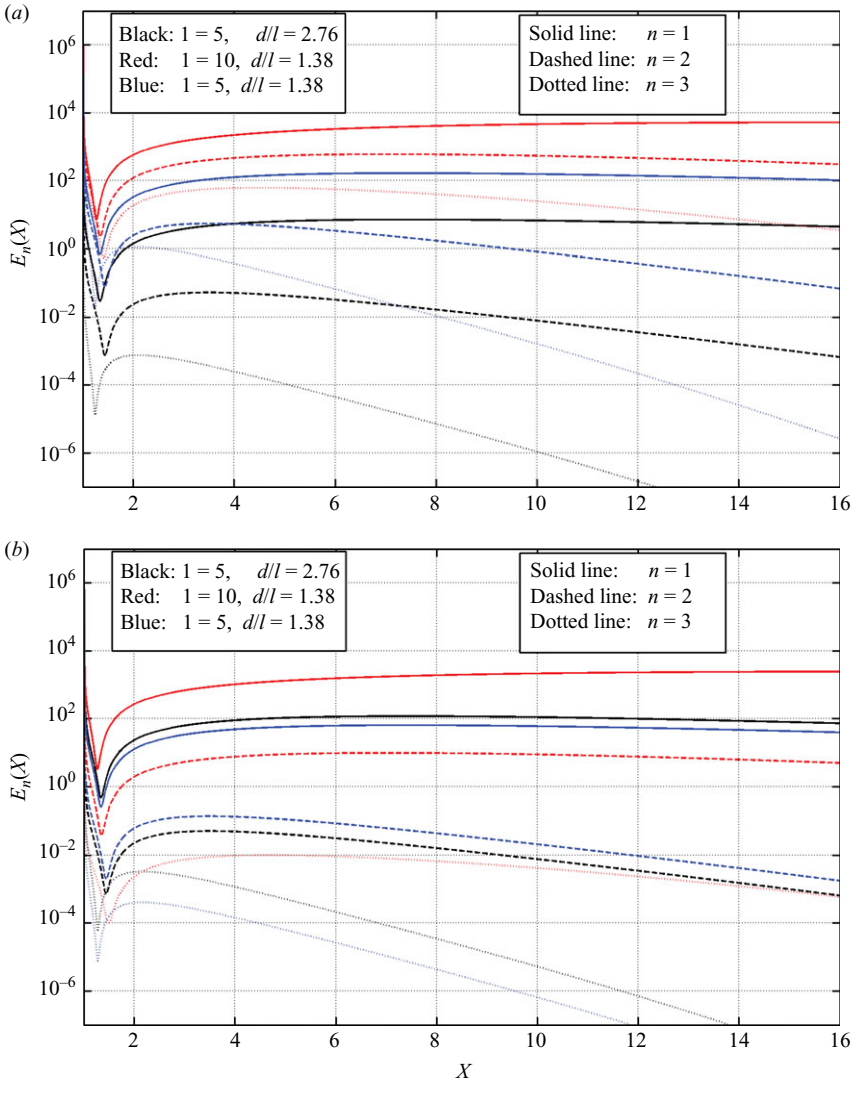

FIGURE 3. Scaled modal energies E_n for $n = 1, 2, 3$ as a function of streamwise variable X, corresponding to (a) Case 1 and (b) Case 2.

Choudhari & Fisher (2005), who performed Navier–Stokes computations for the case $l = 6.57$, $d/l = 2.1$, reported an energy growth factor of $O(300)$ at the relatively large roughness heights of $Re_k = 119$ and 162. It is worth noting that the linear theory predictions are more or less consistent with the simulation results.

While (5.2) shows that the energies will be relatively small in the compact linear case being considered here, figures 3(a) and 3(b) clearly show that the wakes can persist over very long streamwise distances. The persistence of the wakes can also be gauged by the relatively modest values of the decay factor in table 1, which measures the reduction in the modal energy of the fundamental harmonic from its maximum over the interval $x = (1, 5, 16)$ to that at the 'outflow' of this interval ($x = 16$) in figures 3(a) and 3(b).

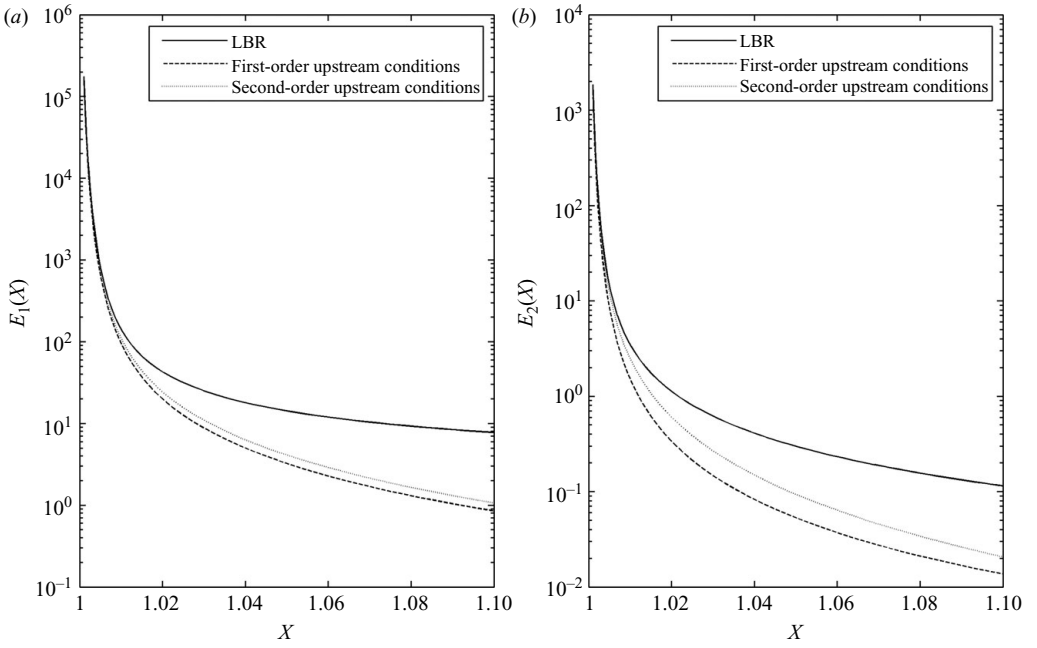

FIGURE 4. Modal energy as a function of streamwise variable X, calculated from the LBR equation solution with the first-order and second-order upstream (a) for first mode and (b) for second mode.

Figure 4 compares the modal energies in the first and second modes computed from the one and two term asymptotic expansions (C 1) to (C 3) of the initial conditions with the corresponding result computed from the full LBR equation solution (with initial conditions computed from the full two term expansion) for Case 1. (The one term expansion corresponds to using only the first square bracketed term in these equations.) It shows, among other things, that there is an 'overlap region' where the LBR solution matches onto the two layer 'inner solution' which describes the flow in the vicinity of the roughness. This region is relatively short and extends downstream to about 1.5 % of the downstream position x_0^* of the roughness for the first mode and about 1 % for the second. The two term expansion shows only slightly better agreement than the one term expansion. The amount of improvement decreases with increasing l/n and only occurs for very small values of $X-1$ when l/n is greater than about 4, i.e. the two term expansion only becomes optimal at very small $X-1$ when l/n is large. Case 2 behaves in a similar fashion.

Figure 5 is a comparison with Choudhari and Fischer's (Choudhari & Fischer 2005) numerical computation of the unscaled modal energies. The agreement appears to be reasonably good for the first mode and relatively poor for the second. But the latter contains very little energy and does not have much effect on the overall accuracy of the computation. The two results show a fair amount of disagreement at smaller values of X, where the numerical solution decays more slowly than the analytical result. This may, at least in part, be due to the fact that only the outer expansion of the analytical solution is plotted here, while the solution at small X is most appropriately described by a composite expansion of the inner and outer solutions which, among other things, would remain finite as $X \to 1$. The discrepancy may also be due to the fact that the nonlinear terms seem to make the inner solution

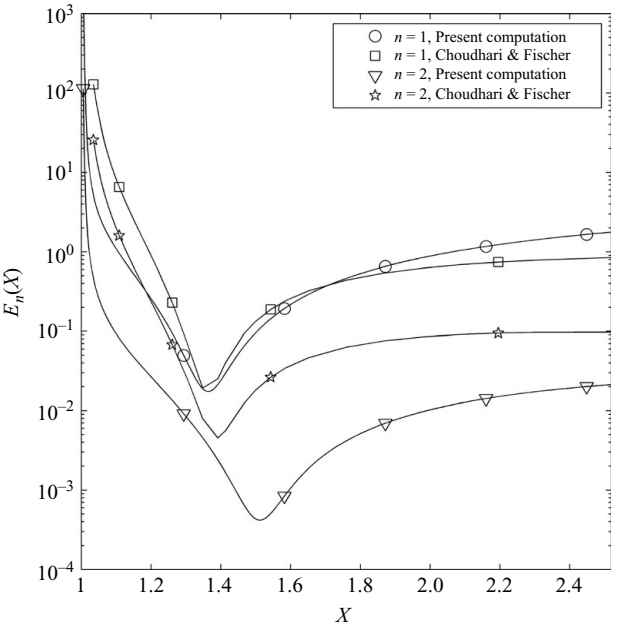

FIGURE 5. Comparison with the numerical solution of Choudhari & Fischer (2005) for $R = 2.5 \times 10^5$, $x_0^* = 230\,\text{mm}$, $l = 6.57$, $d = 13.8$, $h = 1.2$.

decay more slowly even for relatively small values of h (see discussion of nonlinear solution below), or to the fact that the spanwise mean distortion decays out much more slowly than the spanwise variable component – which could contaminate the numerical computations – or it could even be due to the well-known inaccuracy of triple-deck-type computations at moderate Reynolds numbers.

Figures 6 and 7 are plots of the spanwise variable component of the scaled streamwise velocity for Case 1 along the centreline of the elements and along a line half way between the roughness elements respectively. They show that the wakes are initially concentrated in the wall layer but rapidly spread out and move toward the outer edge of the boundary layer as they progress downstream. The figures also show that the velocity defects undergo sign reversals at the downstream locations of the modal energy minima (i.e. at the algebraic growth initiation points) as do the fuller profiles between the elements.

The spanwise variable components of the streamwise velocities for Case 2 are plotted in figures 8 and 9, which show the perturbation profiles along the centreline of the elements and along a line half way between the centrelines of adjacent roughness elements, respectively.

8.2. *The nonlinear problem*

All the computations in this section are based on the smooth roughness shape function (8.5). Figure 10 displays the spanwise variable component of the pressure (normalized with respect to $h\lambda^{5/3}$) calculated from the numerical solutions to the inner boundary-layer problem (3.24)–(3.29) with and without the nonlinear terms. The linear numerical solution is indistinguishable from the analytical result derived in § 6. These results show that pressures increase faster than linearly with increasing h, especially near $x = 0$.

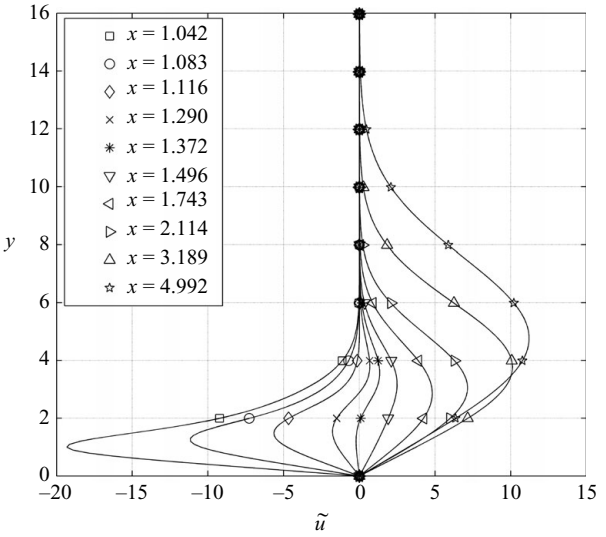

FIGURE 6. Scaled streamwise velocity perturbation $\tilde{u}$ as a function of y for Case 1 at the spanwise location $z = \pi l$ with $l = 5$ and $d/l = 1.38$.

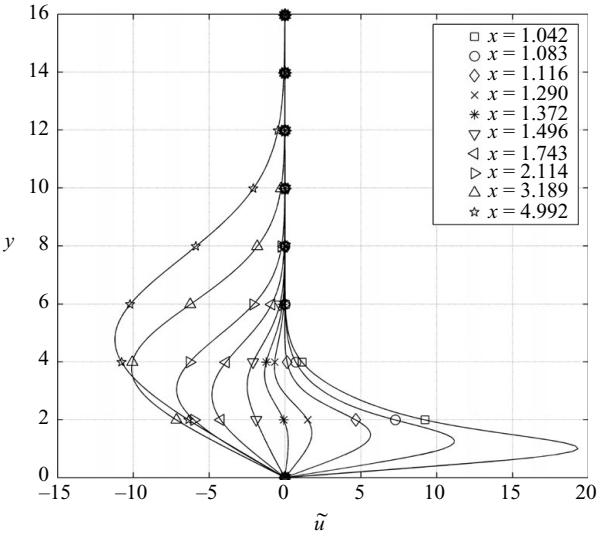

FIGURE 7. Streamwise velocity perturbation $\tilde{u}$ as a function of y for Case 1 at spanwise location $z = 0$ with $l = 5$ and $d/l = 1.38$.

The numerical solutions are also in good agreement with the analytical result when the nonlinear terms are retained if the roughness height h is relatively small – of the order of 0.1 or so. Indeed, the (nonlinear) numerical and linear results are even in good agreement in the vicinity of the roughness for larger values of h – of the order of 1.0 or so. Figure 11 confirms that the numerically computed pressures decay algebraically as $x \to \infty$, but it also shows that the algebraic decay rate α_0 changes from the linear case value of $8/3$ to what appears to be the minimum allowable value of $5/3$ in the fully nonlinear case where $h = O(1)$. The intermediate curves are somewhat ambiguous because they correspond to a superposition of terms with the

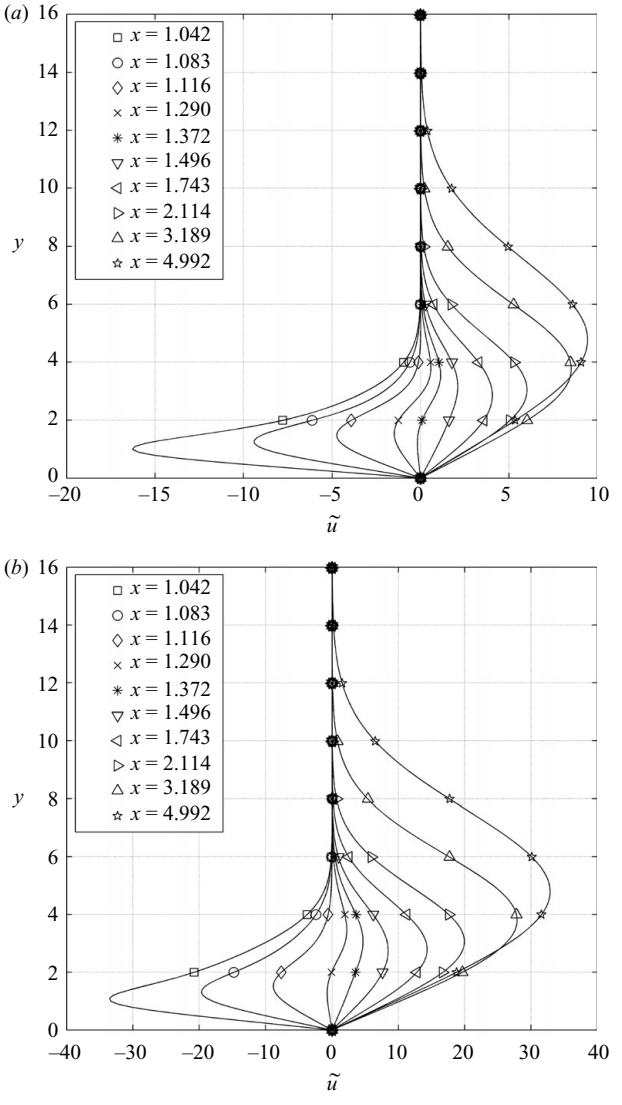

FIGURE 8. Scaled streamwise velocity perturbation $\tilde{u}$ as a function of y for Case 2 at the spanwise location $z = \pi l$. (*a*) $l = 5$ and $d/l = 2.76$ (*b*) $l = 10$ and $d/l = 1.38$.

two different decay rates. The slower decay rate does not emerge until x becomes very large for the smaller values of h. These observations were confirmed by detailed grid studies performed by the authors (but not shown here).

The governing equations are only nonlinear in the vicinity of the roughness elements. But the difference in α_0 between the linear and nonlinear cases (see (5.2)) indicates that the LBR solution for the former (i.e. the strictly linear) case can only remain valid when $X - 1 = O(1)$ if $h \ll \varepsilon^3$ – at least in a strict asymptotic sense. But (5.2) shows that the (unscaled) fully nonlinear modal energies (for $h = O(1)$) will be larger by a factor of $R = \varepsilon^{-6}$ than those in the linear case. This means that even relatively mild nonlinearities in the local inner solution can have a much more significant effect on the far wakes than on the near field flow. This situation is analogous to the acoustic far-field from a source that has been expanded in powers of a small parameter with

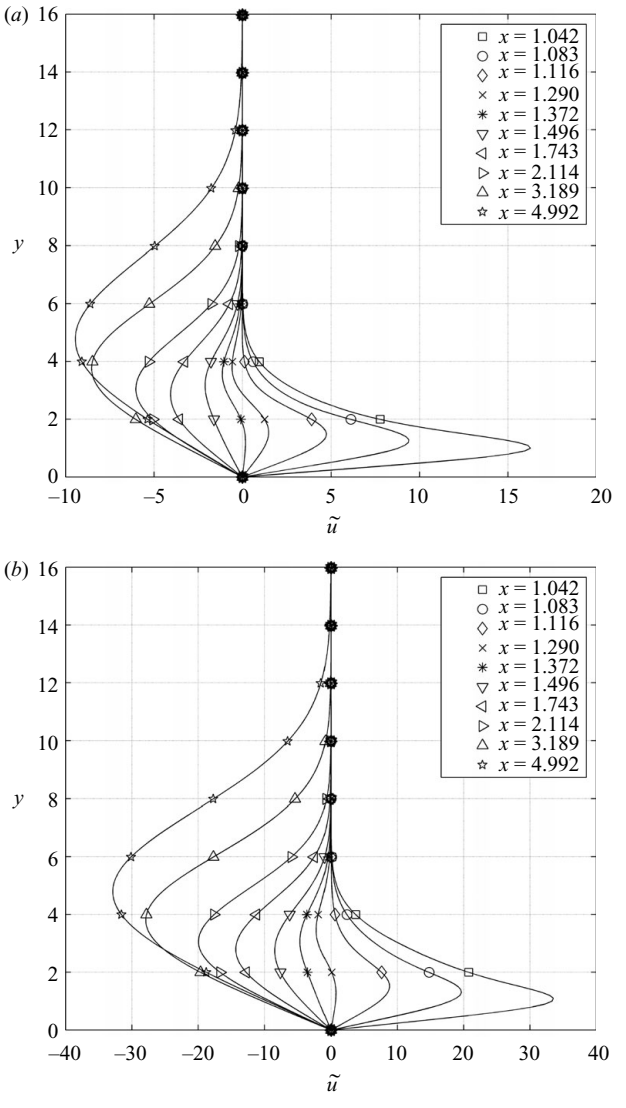

FIGURE 9. Scaled streamwise velocity perturbation $\tilde{u}$ as a function of y for Case 2 at the spanwise location $z=0$. (*a*) $l=5$ and $d/l=2.76$ (*b*) $l=10$ and $d/l=1.38$.

the monopole contribution (which would become the dominant term in the far field) excluded from the lowest order solution (which would correspond to linear solution in the present case) but not from the higher order terms (which would correspond to nonlinear solution).

The distinguished scaling occurs when $h=O(\varepsilon^3)$ and the proper outer expansion of spanwise variable component of the solution (5.2) becomes

$$\begin{aligned}
&\{u, v, w, p\} - \{\bar{u}, \bar{v}, \bar{w}, \bar{p}\} \\
&\quad = \varepsilon^4 h\{\tilde{u}_{(0)}(X, y, z), \delta\tilde{v}_{(0)}(X, y, z), \delta\tilde{w}_{(0)}(X, y, z), \delta^2\tilde{p}_{(0)}(X, y, z)\} \\
&\qquad + \varepsilon h^2\{\tilde{u}_{(1)}(X, y, z), \delta\tilde{v}_{(1)}(X, y, z), \delta\tilde{w}_{(1)}(X, y, z), \delta^2\tilde{p}_{(1)}(X, y, z)\} + \cdots, \\
&\quad = \varepsilon^4 h\{\tilde{u}_{(0)}(X, y, z) + \tilde{u}_{(1)}(X, y, z), \delta[\tilde{v}_{(0)}(X, y, z) + \tilde{v}_{(1)}(X, y, z)], \\
&\qquad \delta[\tilde{w}_{(0)}(X, y, z) + \tilde{w}_{(1)}(X, y, z)], \delta^2[\tilde{p}_{(0)}(X, y, z) + \tilde{p}_{(1)}(X, y, z)]\} + \cdots, \quad (8.10)
\end{aligned}$$

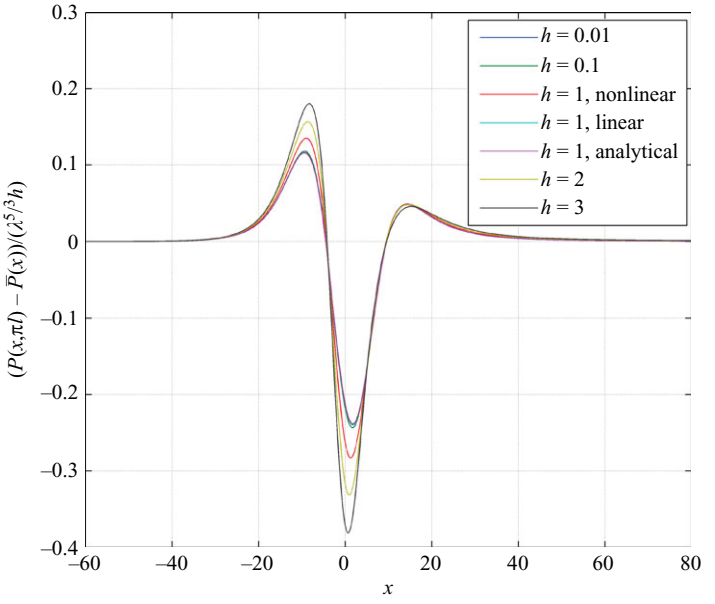

FIGURE 10. Normalized spanwise variable component of surface pressure distribution over the roughness elements for $l = 5$, $d = 6.9$. All results except the $h = 1$ analytic curve are computed from the nonlinear solution.

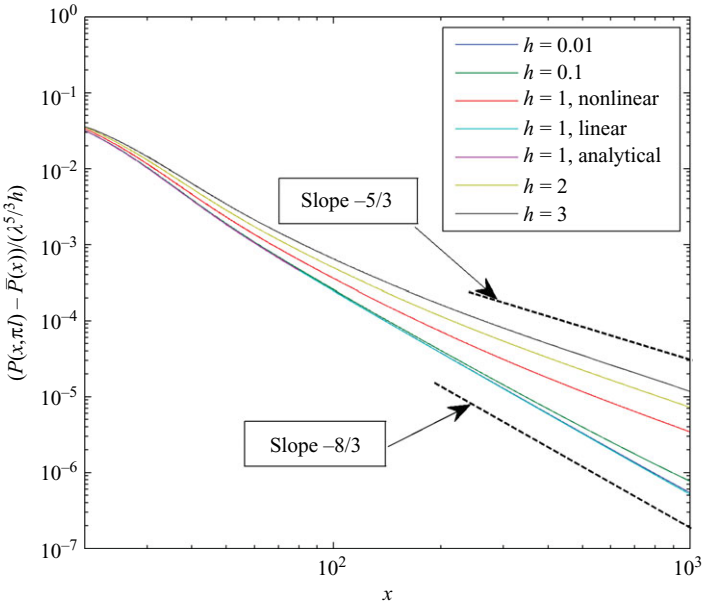

FIGURE 11. Normalized spanwise variable surface pressure decay rates for $l = 5$, $d = 6.9$.

where $\{\tilde{u}_{(0)}, \tilde{v}_{(0)}, \tilde{w}_{(0)}, \tilde{p}_{(0)}\}$ denotes the outer expansion of the linear (inner) solution and $\{\tilde{u}_{(1)}, \tilde{v}_{(1)}, \tilde{w}_{(1)}, \tilde{p}_{(1)}\}$ is the solution of the of the boundary value problem (5.3)–(5.7) that matches onto the dominant component of the nonlinear inner solution as $x \to \infty$, i.e. the solution that behaves like (5.8)–(5.10) with $\alpha = 5/3$ when $X \to 1$ with $y = O(1)$.

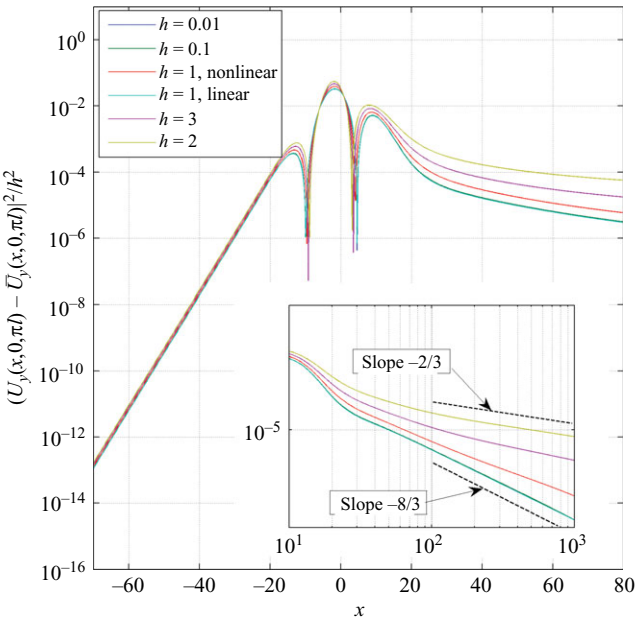

FIGURE 12. Square of the spanwise variable shear stress.

The spanwisevariable component of the streamwise velocity $\varepsilon^4 h\tilde{u}_{(0)}(X, y, z) + \varepsilon h^2\tilde{u}_{(1)}(X, y, z)$ will then behave like

$$\varepsilon^4 h\tilde{u}_{(0)}(X, y, z)+\varepsilon h^2\tilde{u}_{(1)}(X, y, z) \sim \frac{\varepsilon^4 h}{(X-1)^{2/3}}\tilde{u}^{(0)}_{(0),0}(y, z)+\varepsilon h^2(X-1)^{1/3}\tilde{u}^{(0)}_{(1),0}(y, z) \qquad (8.11)$$

as $X \to 1$ with $y = O(1)$, where $\tilde{u}^{(0)}_{(0),0}(y, z)$, $\tilde{u}^{(0)}_{(1),0}(y, z)$ denote the appropriate solutions of (5.11)–(5.13). This suggests that the linear solution modal energy minimum will gradually disappear and a second minimum will emerge at $X - 1 = O(\varepsilon^3/h)$ when $\varepsilon^3 \ll h \ll 1$. There should, therefore, be a range of h for which the modal energies have a double minimum, which has not as yet been observed experimentally – most likely because no experiments have been done for sufficiently small values of h. The remaining minimum should move upstream and disappear into the inner region as $h \to 1$.

To get some sense of its subsequent behaviour, we plotted the square of the spanwise variable shear stress $|U_Y(x, 0, \pi l) - \bar{U}_Y(x, 0, \pi l)|^2$ as a function of x in figure 12. The results show that it only vanishes near the start of the wake region, i.e. in the near field of the roughness array when $x > 0$. This suggests that the streamwise velocity perturbation does not exhibit the wake region sign reversal seen in both the direct Navier-Stokes (DNS) and linear problem LBR computations (see e.g. figures 6 and 9) and, therefore, that the modal energy evolution will not have an easily localized sharp minimum on the short streamwise length scale of the inner region. This is not, however, completely inconsistent with the DNS and linear problem LBR computations since the growth initiation region would still appear to be highly localized on the long streamwise length scale X of the outer region. The insert confirms that the final slopes are entirely consistent with the asymptotic results of § 4.

Equations (3.1) and (3.20) show that the dominant contribution to the total inner region energy (summed over all modes) comes from the wall layer solution with the

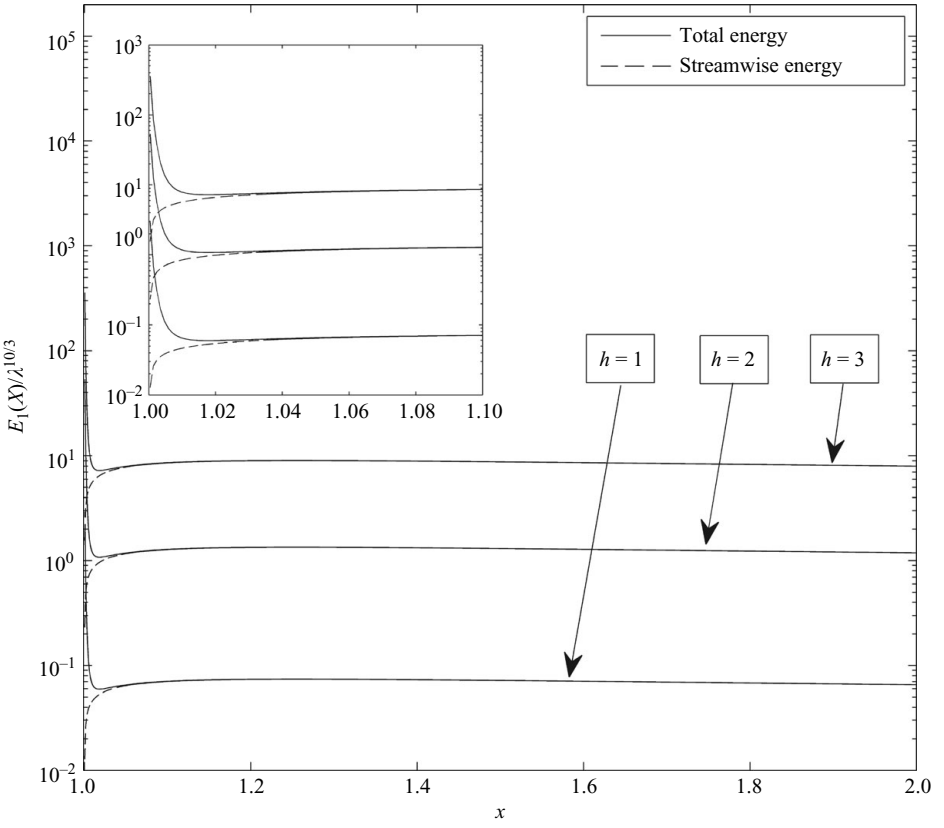

FIGURE 13. Scaled modal energy components of the profile averaged energy for $l = 5$, $d = 6.9$ and $\delta = 1/380$.

crossflow velocities now being just as important as those in the streamwise direction and is given by

$$\varepsilon^3 \int_0^\infty [|U - \lambda \breve{Y}|^2 + |W|^2] \, \mathrm{d}Y. \tag{8.12}$$

This result is smaller than the scaled energies in the outer region by a factor of ε and much larger than the linear solution result, which suggests that nonlinear effects can – order of magnitude wise at least – produce very large wakes in the downstream flow. These results also suggest that the nonlinear effects have an important influence on the far wake behaviour.

Figure 13 is a plot of the scaled modal energy components (8.2) of the profile averaged energy (8.3) and the profile averaged streamwise energy (8.9) for the cases shown in figure 10. We only show the first mode since it contains virtually all of the energy in this case. The figure shows that the sharp energy minimum found in the linear case (figure 3) occurs much further upstream and is much less pronounced in the fully nonlinear problem. The transient energy growth, therefore, appears to be much weaker in this case. But the initial energy decay is now much less severe and the wakes still appear to persist over large streamwise distances. The scaled energy levels are also somewhat smaller than in the linear case but the scale factors (ε^2 as opposed to ε^8) are now much larger.

A uniformly valid high Reynolds number asymptotic solution for the flow over a periodic array of relatively small roughness elements whose spanwise separation is of the order of the local boundary-layer thickness was constructed in this paper. The roughness elements, which are assumed to be more or less circular with streamwise and spanwise scales equal to the local boundary-layer thickness, are required to be small enough to produce only local separation. The analysis shows that there is a local asymptotic ('inner') solution in the vicinity of the roughness elements that decays over a very short streamwise distance, but eventually breaks down in an ('outer') downstream region where the flow is governed by the LBR equations. The solutions to these equations, which continue the local solution into that region, are the main focus of this paper. They can be interpreted as eigensolutions of the LBR equations that often exhibit spatial growth and can persist over relatively long streamwise distances, which are much longer than the distance between the roughness elements and the leading edge.

The 'inner' solution, which is, in general, nonlinear, involves considerable numerical computation. But analytical results were obtained for the strictly linear problem (where the scaled roughness height $h \ll 1$) and extensive numerical computations were carried out for this case. The results show that the outer solution wake energies for the fully nonlinear case (corresponding to $O(1)$ scaled roughness heights) will be larger by a factor of $R = \varepsilon^{-6}$ than those in the strictly linear case. The surprising conclusion from this is that relatively mild nonlinearity ($h = O(1)$ or so) can have a much larger effect on the far wakes than on the near field flow in the vicinity of the roughness.

The second author would like to thank Dr A. Afjeh, Professor and Chairman of the MIME Department, University of Toledo, for his encouraging and valuable support, and Dr R. Hixon, Associate Professor, University of Toledo.

Appendix A

It follows from (3.14) that

$$\pi_0(y,k) = 1 + |k|\pi_0^{(1)}(y) + k^2\pi_0^{(2)}(y) + O(k^3) \quad \text{for } y = O(1), \tag{A 1}$$

where

$$\pi_0(y,k) = \mathrm{e}^{-|k|y} \quad \text{for } |k|y = O(1), \tag{A 2}$$

with $|k| \equiv \lim_{\varepsilon \to 0} \sqrt{k^2 + \varepsilon^2}$ and

$$\pi_0^{(1)} = \int_y^\infty (U_B^2 - 1)\,\mathrm{d}y - y \quad \text{for } y = O(1), \tag{A 3}$$

$$\pi_0 = \frac{1 + |k|\left[\displaystyle\int_y^\infty (U_B^2 - 1)\,\mathrm{d}y - y\right]}{1 + |k|\displaystyle\int_0^\infty (U_B^2 - 1)\,\mathrm{d}y} + O(k^2), \tag{A 4}$$

$$\pi_0(y,0) = 1, \tag{A 5}$$

$$\frac{\mathrm{d}\pi_0^{(1)}}{\mathrm{d}y} = -U_B^2 + \cdots. \tag{A 6}$$

It therefore follows from (3.16) that

$$\pi_0(y,k) = 1 - |k|\frac{\lambda^2 y^3}{3} - k^2\frac{y^2}{2} + O(k^3) \quad \text{as } y \to 0, \tag{A 7}$$

and since

$$\tilde{P}_0^{(j)}(k) \sim (ik)^{\beta_j - 1}\tilde{a}_0^{(j)} \quad \text{as } k \to 0, \tag{A 8}$$

it follows that that

$$\overline{p_j(x,y)} \sim \left[\frac{1}{x^{\beta_j}} + \frac{\beta_j \pi_0^{(1)}(y)}{x^{\beta_j+1}} - \frac{\beta_j(\beta_j+1)\pi_0^{(2)}(y)}{x^{\beta_j+2}} + \cdots\right]\overline{\hat{p}_j}.. \tag{A 9}$$

as $x \to \infty$, and, therefore, from (3.6) and (3.7)

$$\bar{v}_j(x,y) \sim \frac{\lambda\, y\,\overline{\hat{p}_j}}{x^{\beta_j}} - \frac{\beta_j\,\overline{\hat{p}_j}}{\lambda\, x^{\beta_j+1}} + \cdots, \tag{A 10}$$

$$\bar{u}_j(x,y) \sim \frac{\lambda\,\overline{\hat{p}_j}}{(\beta_j - 1)x^{\beta_j - 1}} + \cdots, \tag{A 11}$$

as $y \to 0$, where

$$\bar{\hat{}}p_j(y) \equiv 2\,\sin\pi\beta_j\,\Gamma(\beta_j)\tilde{a}_0^{(j)}. \tag{A 12}$$

Then since $\bar{P}(x)$ and $\bar{P}^{(1)}(x)$ are assumed to decay as $x^{-\beta_i}$ for $i = 0, 2$ as $x \to \infty$, (4.13)–(4.16) will possess solutions of the form

$$\bar{U} - \lambda Y = x^{-(\beta_0+1/3)}\bar{U}_0(\eta), \quad \overline{U^{(1)}} = x^{-(\beta_1+1/3)}\bar{U}_1(\eta) \tag{A 13}$$

and

$$\bar{V} = x^{-(\beta_0+1)}\lambda^{-1/3}\bar{V}_0(\eta),\ \overline{V^{(1)}} = x^{-(\beta_1+1)}\lambda^{-1/3}\tilde{V}_1(\eta, z), \tag{A 14}$$

where $\bar{U}_j$, $\bar{V}_j$ satisfy

$$-\left[\frac{\eta}{3}\frac{\mathrm{d}\bar{U}_j}{\mathrm{d}\eta} + \left(\beta_j + \frac{1}{3}\right)\bar{U}_j\right] + \frac{\mathrm{d}\bar{V}_j}{\mathrm{d}\eta} = 0, \tag{A 15}$$

$$\frac{\mathrm{d}^2\bar{U}_j}{\mathrm{d}\eta^2} + \eta\left[\frac{\eta}{3}\frac{\mathrm{d}\bar{U}_j}{\mathrm{d}\eta} + \left(\beta_j + \frac{1}{3}\right)\bar{U}_j\right] + \frac{\beta_j\overline{\hat{p}_j}}{\lambda^{2/3}} = \bar{V}_j, \tag{A 16}$$

and it follows from (A 10) and (A 11) that they will match with the limiting form of the outer expansion (3.1) if

$$\bar{U}_0 = O(\eta^{-2}), \quad \bar{V}_0 = \frac{\beta_0\overline{\hat{p}_0}}{\lambda^{2/3}} + O(\eta^{-1}), \quad \bar{U}_1 = O(1), \quad \bar{V}_1 = O(\eta), \tag{A 17}$$

provided we take

$$\beta_1 = \beta_0 - 4/3. \tag{A 18}$$

The first-order solution, therefore, grows very rapidly with x and quickly dominates over the zeroeth-order solution. So this solution rapidly breaks down and is probably not very robust at finite Reynolds numbers. In fact it follows from (A 9) that the magnitude of $\varepsilon\,\bar{p}_1$ will be equal to that of $\bar{p}_0$ and the spanwise mean component of the expansion (3.1) will, therefore, break down when $\varepsilon x^{\beta_0-\beta_1} = \varepsilon x^{4/3} = (\delta^{1/4}x)^{4/3} = O(1)$. It is, therefore, necessary to obtain a new expansion in the relatively small 'outer region' where

$$\bar{X} \equiv (x^* - x_0^*)/x_0^*\,\delta^{3/4} = \delta^{1/4}x \tag{A 19}$$

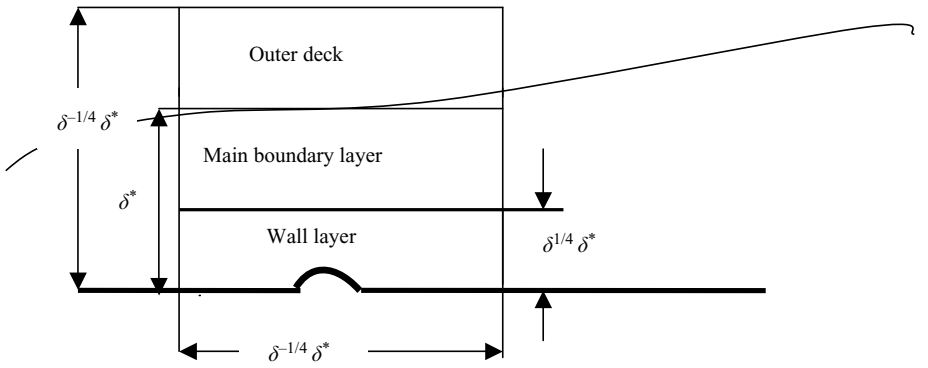

FIGURE 14. Spanwise mean flow structure

is $O(1)$, which is precisely the triple-deck scaling. The flow in this region (depicted in figure 14) is two-dimensional and has the three-layer structure described in § 23.8 of Rothmayer & Smith (1998). Smith (1973) has inferred that the two-dimensional inner solution matches onto an outer linearized triple-deck solution by realizing that the protuberance acts like a delta function on the longer triple-deck length scale (see also Smith *et al.* 1981). He was therefore able to show that $\beta_0 = 2/3$ by considering only the outer solution. He also showed that the solution in the wall layer satisfies the two-dimensional linearized boundary-layer equations (given by (4.11)–(4.13) with $W = 0$) while the solution in the main boundary layer is given by

$$\{u, v, w, p\} = \{U_B(\eta), \delta V_B(X, \eta), 0, 0\} + \varepsilon^2 \delta^{\beta_0/4}\{\delta^{-1/4}\,\bar{\tilde{u}}(\bar{X}, y),\ \bar{\tilde{v}}(\bar{X}, y),\ 0,\ \bar{\tilde{p}}(\bar{X})\}, \tag{A 20}$$

where

$$\bar{\tilde{u}}(\bar{X}, y) = U_B'(y)A(\bar{X}), \qquad \bar{\tilde{v}}(\bar{X}, y) = -U_B(y)\frac{\mathrm{d}A(\bar{X})}{\mathrm{d}\bar{X}} \tag{A 21}$$

and

$$\bar{\tilde{p}}(\bar{X}) \to \frac{\overline{\hat{p}_0}}{\bar{X}^{\beta_0}}, \quad A(\bar{X}) \to a_0\lambda^{2/3}\tilde{F}_0(0) + \frac{\overline{\hat{p}_0}}{i\,(\beta_0 - 1)\bar{X}^{\beta_0 - 1}} \quad \text{as } \bar{X} \to 0 \tag{A 22}$$

with $a_0 = -3(-3Ai'(0)/4)^{3/4}\cos(\pi/8)$, which will clearly match onto (3.1), (A.9), (A.10) and (A.11) if we take

$$\bar{U}_1(y) = a_0\lambda^{2/3}\tilde{F}_0(0), \tag{A 23}$$

when $y = O(1)$. The streamwise velocity perturbation $\bar{U}_1(y)$ is given by the limiting form of the lower-deck solution for $y = O(\delta^{1/4})$.

This solution will itself breakdown on the long streamwise length scale where $X - 1 = O(1)$ and a new outer expansion will have to be obtained. The flow will then be governed by the two-dimensional linearized constant pressure boundary-layer equations. And since Smith (1973) and Smith *et al.* (1981) showed that

$$\bar{\tilde{P}}(\bar{X}) \sim \bar{X}^{-2} \quad \text{and} \quad A(\bar{X}) \sim \bar{X}^{-7/3} \quad \text{as } \bar{X} \to \infty. \tag{A 24}$$

This solution must expand as

$$\{u, v, w, p\} = \varepsilon^3\{(\bar{X}, y),\ \delta\bar{\tilde{v}}(X, y),\ 0, \bar{\tilde{p}}(X, y)\} + \cdots \tag{A 25}$$

for $y = O(1)$.

It now follows from § 6 that the spanwise mean surface pressure is given by

$$\bar{p}_0(x,y) = \int_{-\infty}^{\infty} \pi_0(y,k) \frac{9^{1/3}(\mathrm{i}k\lambda)^{5/3}}{k^2\Gamma(1/3)} \bar{F}_0(k) \mathrm{e}^{\mathrm{i}kx}\,\mathrm{d}k$$

$$\sim -\frac{2\sin\frac{\pi}{3}}{x^{2/3}} \frac{\Gamma(2/3)}{\Gamma(1/3)} 9^{1/3}\lambda^{5/3}\bar{F}_0(0) = -\frac{\sqrt{3}}{x^{2/3}} \frac{\Gamma(2/3)}{\Gamma(1/3)} 9^{1/3}\lambda^{5/3}\bar{F}_0(0) = \frac{\overline{\hat{p}_0}}{x^{2/3}} \quad \text{(A 26)}$$

and

$$\bar{v}_0(x,y) = \frac{1}{U_B(y)} \int_{-\infty}^{\infty} \frac{9^{1/3}(\mathrm{i}k\lambda)^{5/3}}{\mathrm{i}k^3\Gamma(1/3)} \bar{F}_0(k) \frac{\mathrm{d}\pi_0(y,k)}{\mathrm{d}y} \mathrm{e}^{\mathrm{i}kx}\,\mathrm{d}k \sim -\frac{2\sin\frac{\pi}{3}}{x^{2/3}} \frac{\Gamma(2/3)\lambda^{5/3}9^{1/3}U_B(y)}{\Gamma(1/3)}$$

$$\times \bar{F}_0(0) = -\frac{\sqrt{3}}{x^{2/3}} \frac{\Gamma(2/3)\lambda^{5/3}9^{1/3}U_B(y)}{\Gamma(1/3)} \bar{F}_0(0) = \frac{U_B(y)\overline{\hat{p}_0}}{x^{2/3}}. \quad \text{(A 27)}$$

in the linear solution and that $\beta_0 = 2/3$ in this case. Equation (3.6), therefore, shows that

$$\bar{u}_0(x,y) \sim -3U_B'(y)x^{1/3}\overline{\hat{p}_0}, \quad \text{(A 28)}$$

where

$$\overline{\hat{p}_0} \equiv -\frac{\sqrt{3}\Gamma(2/3)}{\Gamma(1/3)} 9^{1/3}\lambda^{5/3}\bar{F}_0(0). \quad \text{(A 29)}$$

Appendix B

$$(3-\alpha+j/3)\tilde{u}_1^{(j)} + \tilde{v}_{1,y}^{(j)} + \tilde{w}_{1,z}^{(j)} = 0, \quad \text{(B 1)}$$

$$(3-\alpha+j/3)U_B(y)\tilde{u}_1^{(j)} + \tilde{v}_1^{(j)}U_B'(y) = \frac{y}{2}F''(y)(2-\alpha+j/3)\tilde{u}_0$$

$$+\frac{1}{2}[yU_B'(y)]'\tilde{v}_0^{(j)} - V_B(1,y)\tilde{u}_{0,y}^{(j)} + \frac{1}{2}yU_B'(y)\tilde{u}_0^{(j)} + \tilde{u}_{0,yy}^{(j)} + \tilde{u}_{0,zz}^{(j)}, \quad \text{(B 2)}$$

$$(2-\alpha+j/3)U_B(y)\tilde{v}_1^{(j)} + \tilde{p}_{1,y}^{(j)} = -\tilde{v}_{0,y}^{(j)}V_B(1,y) - \tilde{v}_0^{(j)}V_{B,y}(1,y) + \tilde{v}_{0,yy}^{(j)} + \tilde{v}_{0,zz}^{(j)}, \quad \text{(B 3)}$$

$$(2-\alpha+j/3)U_B(y)\tilde{w}_1^{(j)} + \tilde{p}_{1,z}^{(j)} = -V_B(1,y)\tilde{w}_{0,y}^{(j)} + \tilde{w}_{0,yy}^{(j)} + \tilde{w}_{0,zz}^{(j)}. \quad \text{(B 4)}$$

Appendix C. Upstream matching conditions for LBR equation solution

In the strictly linear case, the uniformly valid composite expansion of the upstream matching conditions as $X \to 1$ for the LBR equations is given by

$$\tilde{u} \to \frac{1}{(X-1)^{2/3}}\left[\tilde{u}_0^{(0)}(y,z) + \frac{\tilde{U}_0(\eta,z)}{(X-1)^{1/3}} - \frac{9}{10y\lambda}\frac{\partial^2\tilde{p}_0^{(0)}(0,z)}{\partial z^2}\right]$$

$$+\frac{1}{(X-1)^{1/3}}\left[\tilde{u}_0^{(1)}(y,z) + \frac{\tilde{U}_1(\eta,z)}{(X-1)^{1/3}} - \frac{9}{4y\lambda}\frac{\partial^2\tilde{p}_0^{(1)}(0,z)}{\partial z^2} + \frac{3\Gamma(2/3)(3\lambda)^{1/3}}{4\lambda(X-1)^{1/3}}\frac{\partial^2\tilde{p}_0^{(1)}(0,z)}{\partial z^2}\right], \quad \text{(C 1)}$$

$$\tilde{v} \to \frac{1}{(X-1)^{5/3}}\left[\tilde{v}_0^{(0)}(y,z)+\lambda^{-1/3}\tilde{V}_0(\eta,z)-\frac{3}{5\lambda}\frac{\partial^2\tilde{p}_0^{(0)}(0,z)}{\partial z^2}\right]$$

$$+\frac{1}{(X-1)^{4/3}}\left[\tilde{v}_0^{(1)}(y,z)+\lambda^{-1/3}\tilde{V}_1(\eta,z)-\frac{3}{4\lambda}\frac{\partial^2\tilde{p}_0^{(1)}(0,z)}{\partial z^2}+\frac{\Gamma(2/3)(3\lambda)^{1/3}}{2\,\lambda(X-1)^{1/3}}\frac{\partial^2\tilde{p}_0^{(1)}(0,z)}{\partial z^2}y\right], \tag{C 2}$$

$$\tilde{w} \to \frac{1}{(X-1)^{5/3}}\left[\tilde{w}_0^{(0)}(y,z)+\frac{\tilde{W}_0(\eta,z)}{(X-1)^{1/3}}-\frac{3}{5\lambda y}\frac{\partial\,\tilde{p}_0^{(0)}(0,z)}{\partial z}\right]$$

$$+\frac{1}{(X-1)^{4/3}}\left[\tilde{w}_0^{(1)}(y,z)+\frac{\tilde{W}_1(\eta,z)}{(X-1)^{1/3}}-\frac{3}{4\lambda y}\frac{\partial\tilde{p}_0^{(1)}(0,z)}{\partial z}\right], \tag{C 3}$$

$$\tilde{p} \to \frac{\tilde{p}_0^{(0)}(y,z)}{(X-1)^{8/3}}+\frac{\tilde{p}_0^{(1)}(y,z)}{(X-1)^{7/3}} \tag{C 4}$$

with the relevant quantities given by (4.3), (4.22), (4.39), (4.40) and (5.24)–(5.26).

REFERENCES

Abramowitz, M. & Stegun, I. A. 1965 *Handbook of Mathematical Functions*. National Bureau of Standards.

Acarlar, M. S. & Smith, C. R. 1987 A study of hairpin vortices in a laminar boundary layer. Part 1. *J. Fluid Mech.* **175**, 1–42.

Andersson, P., Berggren, M. & Henningson, D. S. 1999 Optimal disturbances and bypass transition in boundary layers. *Phys. Fluids* **11** (1), 134–150.

Berry, S. A., Auslender, A. H., Dilley, A. D. & Calleja, J. F. 2001 Hypersonic boundary-layer trip development for hyper-X. *J. Spacecr. Rockets* **38** (6), 853–864.

Butler, K. M. & Farrell, B. F. 1992 Three-dimensional optimal perturbations in viscous shear flow. *Phys. Fluids* A **4** (8), 1637–1650.

Carrier, G. F., Krook, M. & Pearson, C. E. 1966 *Functions of a Complex Variable*. McGraw-Hill.

Case, K. M. 1960 Stability of plane couette flow. *Phys. Fluids* **3**, 143–148.

Choudhari, M. & Duck, P. W. 1996 Nonlinear excitation of inviscid stationary vortex instabilities in boundary layer flow in IUTAM symposium on nonlinear instability and transition in three-dimensional boundary layers. In *Proceedings of the IUTAM Symposium*, Manchester, UK, 17–20 July 1995 (ed. P. W. Duck & P. Hall). Kluwer Academic Publishers.

Choudhari, M. & Fischer, P. 2005 Roughness induced transient growth. Presented at the Thirty-fifth AIAA Fluid Dynamics Conference and Exhibit. *AIAA Paper 2005-4765*.

Choudhari, M., Li, F. & Edwards, J. A. 2009 Stability analysis of roughness array wake in a high-speed boundary layer. *AIAA Paper 2009-0170*.

Cossu, C. & Brandt, L. 2002 Stabilization of Tollmien–Schlichting waves by finite amplitude optimal streaks in the Blasius boundary layer. *Phys. Fluids* **14**, L57–L60.

Denier, J. P., Hall, P. & Seddougui, S. O. 1991 On the receptivity problem for Görtler vortices': vortex motions induced by wall roughness. *Phil. Trans. R. Soc. Lond.* A **335**, 51–85.

Ellingson, T. & Palm, E. 1975 Stability of linear flow. *Phys. Fluids* **18**, 487–488.

Farrell, B. F. 1988 Optimal excitation of perturbations in viscous shear flows. *Phys. Fluids* **31**, 2093–2102.

Fransson, J. H. M., Brandt, L., Talamelli, A. & Cossu, C. 2004 Experimental and theoretical investigation of the non-modal growth of steady streaks in a flat plate boundary layer. *Phys. Fluids* **16**, 10, 3627–3638.

Fransson, J. H. M., Brandt, L., Talamelli, A. & Cossu, C. 2005 Experimental study of the stabilization of Tollmien–Schlichting waves by finite amplitude streaks. *Phys. Fluids* **17**, 054110–15.

Gaster, M., Grosch, C. E. & Jackson, T. L. 1994 The velocity field created by a shallow bump in a boundary layer. *Phys. Fluids* **6** (9), 3079–3085.

Goldstein, M. E. 1985 Scattering of acoustic waves into Tollmien–Schlichting waves by small streamwise variations in surface geometry. *J. Fluid Mech.* **154**, 509–529.

Goldstein, M. E. & Hultgren, L. 1989 Boundary-layer receptivity to long-wave free-stream disturbances. *Annu. Rev. Fluid Mech.* **21**, 137–166.

Goldstein, M. E. & Sescu, A. 2008 Boundary-layer transition at high free-stream disturbance levels – beyond Klebanoff modes. *J. Fluid Mech.* **613**, 95–124.

Harlow, F. H. & Welch, J. E. 1965 Numerical calculation of time-dependent viscous incompressible flow of fluid with free surfaces. *Phys. Fluids* **8**, 2182–2189.

Kemp, N. H. 1951 The laminar three-dimensional boundary layer and the study of the flow past a side edge. MAes Thesis, Cornell University, Ithaca, NY.

Kendall, J. M. 1982 Laminar boundary layer distortion by surface roughness: effect upon stability. Part II. Air Force Wright Aeronautic Labratories Report, AFWAL-TR-82–3002.

Kendall, J. M. 1985 Experimental study of disturbances produced in a pre-transitional laminar boundary layer by weak free-stream turbulence. *AIAA Paper 85-1695.*

Klebanoff, P., Cleveland, W. G. & Tidstrom, K. D. 1992 On the evolution of a turbulent boundary layer induced by a three-dimensional roughness element. *J. Fluid Mech.* **237**, 101–187.

Landahl, M. T. 1980 A Note on an algebraic instability of inviscid parallel shear flows. *J. Fluid Mech.* **98**, 243–251.

Leib, S. J. Wundrow, D. W. & Goldstein, M. E. 1999 Effect of free-stream turbulence and other vortical disturbances on a laminar boundary layer. *J. Fluid Mech.* **380**, 169–203.

Levin, P. & Henningson, D. S. 2003 Exponential vs. algebraic growth and transition prediction in boundary layer flow. *Flow Turbul. Combust.* **70**, 183–210.

Luchini, P. 2000 Reynolds-number-independent instability of the boundary layer over a flat surface: optimal perturbations. *J. Fluid Mech.* **404**, 289–309.

Reshotko, E. 2001 Transient growth — a factor in bypass transition. *Phys. Fluids* **13** (5), 1067–1075.

Reshotko, E. & Tumin, A. 2002 Investigation of the role of transient growth in roughness-induced transition. *AIAA Paper 2002-2850.*

Rothmayer, A. P. & Smith, F. T. 1998 *Incompressible Triple Deck Theory, The Handbook of Fluid Dynamics.* CRC Press.

Smith, F. T. 1973 Laminar flow over a small hump on a flat plate. *J. Fluid Mech.* **57**, 803–824.

Smith, F. T. 1976*a* Flow through constricted pipes and channels. Part 1. *Quart. J. Mech. Appl. Math.* **29**, 343–364.

Smith, F. T. 1976*b* Flow through constricted pipes and channels. Part 2. *Quart. J. Mech. Appl. Math.* **29**, 365–376.

Smith, F. T. 1991 Steady and unsteady three-dimensional interactive boundary layers. *Comput. Fluids* **20** (3), 243–268.

Smith, F. T., Brighton, P. S., Jackson, P. S. & Hunt, J. C. R. 1981 On boundary layer flow over two-dimensional obstacles. *J. Fluid Mech.* **113**, 123–152.

Tani, I., Komoda, H., Komatsu, Y. & Iuchi, M. 1962 Boundary-layer transition by isolated roughness. Report 375. Aeronautical Research Institute, University of Tokyo.

Tannehill, J. C., Anderson, D. A. & Pletcher, R. H. 1997 *Computational Fluid Mechanics and Heat Transfer*. Taylor & Francis.

Trefethen, L. N., Trefethen, A. E., Reddy, S. C. & Driscoll, T. A. 1993 Hydrodynamic Stability without Eigenvalues. *Science* **261**, 578–584.

Tumin, A. & Reshotko, E. 2001 Spatial theory of optimal disturbances in boundary layers. *Phys. Fluids* **13** (7), 2097–2104.

Tumin, A. & Reshotko, E. 2005 Receptivity of a boundary-layer flow to a three-dimensional hump at finite Reynolds numbers. *Phys. Fluids* **17** (9), 094101-094101-8.

Westin, K. J. A., Boiko, A. V., Klingmann, B. G. B., Kozlov, V. V. & Alfredsson, P. H. 1994 Experiments in a boundary layer subjected to free-stream turbulence. Part 1. Boundary layer structure and receptivity. *J. Fluid Mech.* **281**, 193–218.

White, E. B. & Ergin, F. G. 2003 Receptivity and transient growth of roughness-induced disturbances. *AIAA Paper 2003-4243.*